



ORIGINAL ARTICLE

Electrochemical behavior and interfacial bonding mechanism of new synthesized carbocyclic inhibitor for exceptional corrosion resistance of steel alloy: DFTB, MD and experimental approaches



Abdelkarim Chaouiki ^{a,1}, Maryam Chafiq ^{a,1}, Aisha H. Al-Moubaraki ^b,
Mohamed Bakhouch ^c, Mohamed El Yazidi ^d, Young Gun Ko ^{a,*}

^a Materials Electrochemistry Laboratory, School of Materials Science and Engineering, Yeungnam University, Gyeongsan 38541, Republic of Korea

^b Department of Chemistry, Faculty of Sciences–Alfaisaliah Campus, University of Jeddah, Jeddah, Saudi Arabia

^c Laboratory of Bioorganic Chemistry, Department of Chemistry, Faculty of Sciences, Chouaib Doukkali University, P.O. Box 24, 24000 El Jadida, Morocco

^d University Sidi Mohamed Ben Abdellah, Faculty of Sciences Dhar EL Mahraz, Engineering Laboratory of Organometallic and Molecular Materials and Environment, P.O. Box 1796 (Atlas), 30000 Fez, Morocco

Received 13 June 2022; accepted 28 September 2022

Available online 3 October 2022

KEYWORDS

Corrosion inhibitor;
Electron transfer behavior;
Interfacial mechanism;
Electronic-/atomic-scale
calculations

Abstract A new carbocyclic compound, namely 3-benzoyl-4-hydroxy-4-phenyl-2,6-(4-methylphenyl)cyclohexane-1,1-dicarbonitrile (MPC) was synthesized and characterized. Herein, MPC was used as green compounds and its anti-corrosion performance was evaluated on the basis of singular role of electron donor–acceptor of MPC molecule. For this purpose, a combination of experimental studies and electronic-/atomic-scale calculations were performed in a bid to understand the electrochemical behavior and interfacial mechanism of MPC molecule based on the correlation between electron charge transfer and adsorption mechanism. Theoretical perspectives are also used to validate the significant inhibition feature achieved by the experimental studies and propose a mechanism of adsorption by using density functional theory (DFT) and molecular dynamic (MD) simulations. According to DFT and MD perspectives, it is found that MPC presents strong interaction with metal surface due to its considerable ability to provide lone pair electrons for

* Corresponding author.

E-mail address: younggun@ynu.ac.kr (Y.G. Ko).

¹ These authors contributed equally to this work.

Peer review under responsibility of King Saud University.



Production and hosting by Elsevier

electrophilic attacks. This is demonstrated by the high adsorption energy (-5.83 eV) and the parallel configuration of MPC which reveal the formation of molecular self-assembly triggered by an organic-surface interaction. The reliable corrosion stability was provided for 72 h of immersion at an optimum concentration with a fairly high inhibition efficiency (85.81 %) due to the formation of organic inhibitive layer. The addition of MPC inhibitor worked as a sealing agent to reduce the corrosion rate, thus forming a dense and protective barrier on the metal surface. The corrosion resistance of mild steel sample was enhanced significantly due to a high adsorption ability arising from the electron-rich nature of molecule. The formation of organic layer on the metal surface was discussed in relation to the intermolecular interactions and microstructural observations by considering the charge transfer behavior responsible for exceptional corrosion protection of steel alloys. The computational simulations were consistent with the experimental results and confirm the importance of developing eco-friendly hybrid materials.

© 2022 The Author(s). Published by Elsevier B.V. on behalf of King Saud University. This is an open access article under the CC BY-NC-ND license (<http://creativecommons.org/licenses/by-nc-nd/4.0/>).

1. Introduction

As a widespread problem, the consequences of environmental corrosion are a key public health issue of the 21st century. It causes substantial economic damage and catastrophic harm, such as damage to crops, infrastructure, daily life, and businesses (Migahed et al., 2018). Metal degradation is expected to cost \$2.5 trillion per year globally (Topçu and Uzunömeroğlu, 2020). The phenomenon of metal corrosion occurs when metals come into contact with certain substances in the environment, resulting in the total or partial degradation of the metal by losing its properties (Dararatana et al., 2018). A phenomenon that is inevitable and unavoidable.

Today's available strategies, such as providing a physical barrier or deliberately controlling the corrosion reaction, are inappropriate and impractical. This context leads to the use of corrosion inhibitors as an alternative. Corrosion inhibitors are available in a multitude of sizes and forms (Antonićević and Petrović, 2008). For instance, organic compounds have acquired favor as metal corrosion inhibitors due to their properties such as their effectiveness in a wide range of temperatures, compatibility with protected materials, and good solubility (Dariva and Galio, 2014). However, several studies (Chigondo and Chigondo, 2016; Singh and Bockris, 1996; Stupnišek-Lisac et al., 2002, 1998; Zaferani et al., 2013) have shown that many products are toxic and therefore not environmentally friendly. As ecological and environmental precautionary awareness has continued to be a major concern, environmentally friendly alternative treatments are being discovered in all aspects of research and technology, with an emphasis on the area of metal corrosion inhibition. For this purpose, it is necessary to implement a new and innovative technique based on ecological corrosion inhibitors (CIs). This type of approach is considered the best in many construction industries, such as automotive, military, real estate, and marine applications. Where mild steel (MS) is widely used due to its excellent mechanical strength, physical characteristics and durability, and especially in the presence of the most commonly used agents for pickling and chemical cleaning such as HCl, which leads to the degradation of metals through the phenomenon of corrosion (Obot et al., 2020; Solmaz, 2010; Tian et al., 2017; Zhang and Cheng, 2009).

As a general rule, the inhibition of metals occurs by the adsorption of inhibitors on the metallic surfaces to be protected, with the formation of a protective layer on the surface (Assad and Kumar, 2021; Verma et al., 2021a). Many aspects affect the degree of adsorption, such as the nature of the metals, the electrolyte medium, the environmental thermality, the nature of the replacement, the structure of the electronic inhibitor, like the density of the donors, and the solubility of the inhibitor, etc. (El-Sayed, 2007; Mofidabadi et al., 2022; Onyechu et al., 2019; Qiang et al., 2021; Sherif and Park, 2006). Considering the necessity of corrosion inhibition by using organic compounds as green corrosion inhibitors, and due to their non-toxic

qualities and the insignificant damage to surrounding ecosystems, carbocyclic compounds appear to be a suitable choice as a replacement for current harmful corrosion inhibitors.

Under this investigation, 3-benzoyl-4-hydroxy-4-phenyl-2,6-(4-methylphenyl)cyclohexane-1,1-dicarbonitrile (MPC) was, for the first time, synthesized and investigated as an environmentally friendly and durable corrosion inhibitor for MS in a 1 M HCl corrosive medium. As far as the authors are aware, there has been no documented protection of MS surfaces with MPC compound in 1 M HCl medium, considered among the most aggressive corrosive media. Therefore, to evaluate the inhibition performance of MPC, weight loss method (WL), electrochemical impedance spectroscopy (EIS), potentiodynamic polarization measurement (PDP) techniques, and scanning electron microscopy (SEM/EDS) were performed in this paper. In addition, more details about the mechanism of adsorption of the studied compound on a Fe surface have been determined through the calculations of the adsorption parameters at the atomic scale and the corresponding electronic impacts have been carried out according to the density functional theory (DFT) method and molecular dynamics (MD) simulations.

2. Experimental section

2.1. Synthesis of 3-benzoyl-4-hydroxy-4-phenyl-2,6-(4-methylphenyl)cyclohexane-1,1-dicarbonitrile

All chemicals are of analytical grade and are used as purchased from commercial suppliers. The melting point is determined using the KOFER Bench apparatus. An infrared spectrum was recorded on a BRUKER VERTEX70 FT-IR spectrometer. ¹H NMR and ¹³C NMR spectra were recorded on the BRUKER AVANCE IITM 300 MHz Ultra-Shield system using CDCl₃ as the solvent and TMS as the internal standard. Chemical shifts δ are expressed in ppm and proton coupling constants J are reported in hertz (Hz). The spin multiplicities are reported as singlet (s), doublet (d), doublet of doublets (dd), triplet (t), doublet of triplets (dt), and multiplet (m). The 4-methylchalcone used as synthons was prepared according to a known procedure (Jacobsen, 2016).

3-benzoyl-4-hydroxy-4-phenyl-2,6-(4-methylphenyl)cyclohexane-1,1-dicarbonitrile (MPC).

In a 100 mL two-necked flask equipped with a condenser and a dropping funnel. We introduce 2 mol of 4-methylchalcone into 30 mL of ethanol and 1 mL of piperidine. Then, a solution of 1 mol of malononitrile in 2 mL of ethanol was added drop by drop. The mixture was refluxed until the

consumption of the synthons, as evidenced by TLC. The solvent was distilled off using a rotary evaporator and the residue was crystallized in ethanol to obtain a whitish solid (yield = 85 %; m.p. = 212–214 °C).

IR (neat, ν in cm^{-1}): 3412 (O—H), 1644 (C=O). ^1H NMR (300 MHz, CDCl_3 , δ in ppm): 2.16 (s, 3H, $-\text{CH}_3$), 2.26 (dd, 1H, H^b , $J_1 = 14.4$ Hz, $J_2 = 3.3$ Hz), 2.37 (s, 3H, $-\text{CH}_3$), 2.93 (dt, 1H, H^c , $J_1 = 15.0$ Hz, $J_2 = 2.4$ Hz), 4.17 (dd, 1H, H^d , $J_1 = 12.7$ Hz, $J_2 = 3.0$ Hz), 4.18 (d, 1H, H^e , $J = 11.9$ Hz), 4.84 (d, 1H, H^f , $J = 11.9$ Hz), 5.16 (d, 1H, H^a , $J = 2.1$ Hz), 6.93 (d, 2H, H_{ar} , $J = 8.4$), 7.07–7.18 (m, 3H, H_{ar}), 7.21–7.28 (m, 4H, H_{ar}), 7.32 (dd, 2H, H_{ar} , $J = 8.1$), 7.38 (dd, 3H, H_{ar} , $J_o = 8.8$ Hz, $J_m = 1.8$ Hz), 7.47 (d, 2H, H_{ar} , $J_o = 7.9$ Hz), 7.54 (d, 2H, H_{ar} , $J_o = 8.3$ Hz). ^{13}C NMR (75 MHz, CDCl_3 , δ in ppm): 20.95 ($\underline{\text{C}}\text{H}_3$), 21.13 ($\underline{\text{C}}\text{H}_3$), 40.72 (C_5), 45.78 (C_6), 48.40 (C_1), 49.85 (C_2), 51.69 (C_3), 74.56 (C_4), 113.88, 127.72, 128.03, 128.09, 128.51, 128.65, 129.33, 129.58, 130.65, 133.49, 133.53, 137.29, 138.89, 139.05, 143.92, 204.13 (C=O).

2.2. Materials and reagents

The specimens of MS with the following composition (wt. %): 0.370 % C, 0.230 % Si, 0.680 % Mn, 0.016 % S, 0.077 % Cr, 0.011 % Ti, 0.059 % Ni, 0.009 % Co, 0.160 % Cu and the balance Fe were used as the samples for the current study. Before any measurement, the samples were sanded and smoothed using 200 to 1800 series emery paper, washed with distilled water, and then air dried. All corrosion experiments were performed in 1 M HCl, which had previously been prepared from HCl stock (37 % reagent grade). The inhibitor concentrations that were utilized in this study were 10^{-6} , 10^{-5} , 10^{-4} , and 10^{-3} M of MPC compound in 1 M HCl solution.

2.3 wt. loss (WL) measurement

To perform the WL tests, the steel was cut into sheets of dimensions ($2 \times 1.5 \times 0.2$) cm^3 from a wide strip. The samples were then polished with emery sheets before being sonicated in 50 % ethanol, dried and stored in a desiccator. For each of the tested temperatures varying from 303 K to 333 K, the solution was thermally controlled. Following the 24-hour soaking process, the steel specimens were removed from the test solution, the corrosion products were removed, properly cleaned with demineralized water, dried, and accurately reweighed. All these tests were used in triplicate, and the standard deviation for the three measurements was calculated. To calculate the corrosion rate, inhibition efficiency and surface coverage, gravimetric results with and without MPC have been employed. They are calculated according to the equations below:

$$C_R = \frac{8.76 \times \Delta W}{D \times A \times t} \quad (1)$$

$$\eta_{WL}(\%) = \left[1 - \frac{C_R}{C_R^0}\right] \times 100 \quad (2)$$

$$\theta = \frac{C_R^0 - C_R}{C_R^0} \quad (3)$$

Here, ΔW denotes the weight loss (mg), A is the area of MS specimens (cm^2), t = exposure time (h), D = density of steel specimens (g cm^{-3}), C_R and C_R^0 represent the corrosion rates with various inhibitor concentrations and in blank, while θ is the degree of surface coverage.

2.4. Electrochemical assessment

In this study, tri-electrodes cell containing an Ag/AgCl, platinum and mild steel have been used respectively as reference, counter, and working electrodes. The working electrode was embedded in Teflon using epoxy resin, giving a constant surface area of 1 cm^2 , which is exposed to the tested solutions. Prior the electrochemical measurements, the working electrode was polished, cleaned, and allowed to dry at the beginning of each run. All the electrochemical corrosion measurements were performed using a Volta lab potentiostat / galvanostat of the type Corrtest Instruments Corp, ltd. (Wuhan, China). The EIS tests have been carried out at an open circuit potential (OCP) with an AC amplitude of 5 mV over a frequency range of 100 KHz to 10 mHz, and the results have been modeled using ZView software. The PDP tests have been performed at a scan rate of 1 mV/s and a potential range of -800 to -200 mV vs E_{OCP} . Before the electrochemical corrosion experiments, and in order to achieve free corrosion potentials, the specimens were maintained in immersion for 30 min in the electrolyte. The working temperature was 303 ± 1 K. For each experimental condition, all measurements were performed in triplicate to confirm the reliability and reproducibility of the results, and the mean values of the data were recorded.

The protective ability in term of inhibition performance is evaluated from EIS measurements using the following formula (Gerengi and Sahin, 2012):

$$\eta_{EIS}(\%) = \frac{R_p^{inh} - R_p^0}{R_p^{inh}} \times 100 \quad (4)$$

R_p^0 and R_p^{inh} are the polarization resistance without and with the addition of inhibitor compound, respectively.

The corrosion inhibition efficiency was evaluated from PDP measurements according to the following equation (Desimone et al., 2011):

$$\eta_{PDP}(\%) = \frac{i_{corr}^0 - i_{corr}}{i_{corr}^0} \times 100 \quad (5)$$

Where i_{corr}^0 and i_{corr} represent respectively the corrosion current density without and with the addition of inhibitor compound.

2.5. Surface morphology studies

After submerging the MS for 72 h without and with optimal concentration of MPC, Scanning Electron Microscopy (SEM) equipped with Energy-Dispersive X-ray Spectroscopy (EDS) analysis was applied for image interpretation using SEM model-Hitachi TM-1000 (recorded at a magnification of around 1000). Prior to SEM and EDS morphological analysis, the surface of the specimens experienced a similar pre-treatment as previously described in weight loss and

electrochemical testing. The EDS spectrum was also examined in order to investigate and offer details on the elemental components of the layer generated on mild steel during the corrosion inhibition process.

2.6. Theoretical details and models

A key to answering the question of the molecular mechanism behind corrosion inhibition can be easily understood through the quantum chemical properties (QC) and interfacial behavior of the MPC /MS system. This can provide a valuable tool to better understand adsorption processes and their related electronic impacts. By applying density functional theory (DFT), tight binding (DFTB), and molecular dynamics (MD), many levels of theory are applied to highlight and correlate the molecular characteristics of MPC with its adsorption mechanism, using the advanced principles of theoretical chemistry. The Gaussian 16 W software was used to model, provide optimized configuration, and further compute the electronic stability of the molecule under study in the aqueous phase defined in the SMD model. The functional B3LYP/6-311G++(d,p) and the ground state computation have been included below the DFT parameter in order to get the entry record. To validate the experimental insights, the highest occupied molecular orbital energy (HOMO), the lowest unoccupied molecular orbital energy (LUMO), and the energy gap (ΔE) have been recognized for deriving the various overall reactivity properties as: the electron affinity (A), ionization potential (I), electronegativity (χ), hardness (η), softness (σ), electrophilicity (ω), and fraction of transferred electrons (ΔN) as detailed elsewhere (Chafiq et al., 2021a, 2021b). Several other functions were also researched, and their results were compared with the above-mentioned experimental observations. These functions include the density of states (DOS), the electron localization function (ELF), and the electrostatic potential (ESP). The Multiwfn program was used for electronic wavefunction analysis, and VMD software was performed for detailed visualization of the molecular systems (Lu and Chen, 2012) (Humphrey et al., 1996).

On the other hand, in view of looking at the interfacial behavior of the inhibitor molecule being investigated on the metal surface, the DFTB method has been adopted (Aradi et al., 2007). In this case, the code DFTB⁺ available in the Material Studio software package, was used for all the DFTB simulations. This was done through the use of the trans3d Slater–Koster library (Zheng et al., 2007) coupled to a self-consistent charge (SCC) formalism for empirical dispersion correction (Elstner et al., 1998). The optimization of each model includes the following factors: SCC tolerance of 0.05 kcal mol⁻¹ for energy, 0.5 kcal mol⁻¹ Å⁻¹ for force, and max. displacement of 0.001 Å. The adsorption energy (E_{ads}) of a chemical interaction involving a particular iron surface and a defined inhibitor is calculated from the following equation (Musa et al., 2012):

$$E_{ads} = E_{surf+inh} - (E_{surf} + E_{inh}) \quad (6)$$

where $E_{surf+inh}$ is the total energy of the inhibitor/Fe(110), E_{surf} the energy of clean iron slab, and E_{inh} the energy of the inhibitor.

The MD calculations of the corrosion systems composed of mild steel metal and corrosion inhibitor structure were con-

structed by the Forcite module in Materials Studio software. The metallic structure Fe (110) was chosen according to its stability because of its lower energy, which is in the order Fe (110) < Fe(100) < Fe(111). Then, a periodic structure made of Fe(110) and a 39.93 Å × 39.93 Å × 77.04 Å simulation box with a 10 × 10 iron plate, an aqueous phase (H₂O, H₃O⁺, Cl⁻, inhibitor molecule), and a vacuum layer were created. Furthermore, the COMPASS II force field is used to simulate the MD systems, with an NVT ensemble at 298 K with a fine computational accuracy and a simulation time of 5000 ps with a step time of 1 fs. For this level of theory, the interplay between the organic compound and the metal interface in a corrosive medium is predicted according to the formula given below:

$$E_{inter} = E_{total} - (E_{surf+sol} + E_{inh+sol}) + E_{sol} \quad (7)$$

where E_{total} is the simulated total energy of the system, $E_{surf+sol}$ refers to the simulated energy of iron slab and solution, and E_{sol} means the solution energy inside the studied system.

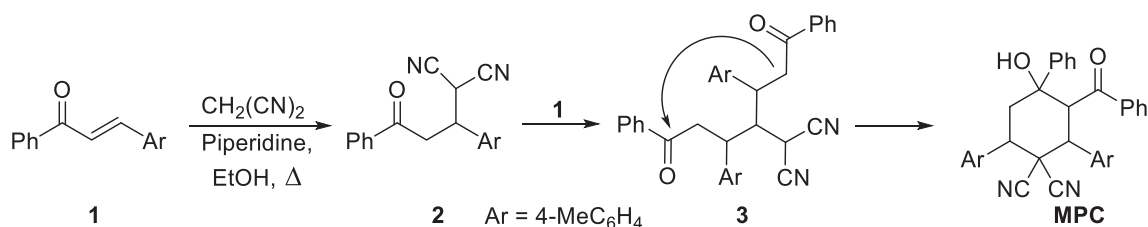
3. Results and discussion

3.1. Synthesis and characterization of MPC compound

The 3-benzoyl-4-hydroxy-4-phenyl-2,6-(4-methylphenyl)cyclohexane-1,1-dicarbonitrile was obtained by the action of malononitrile on 4-methylchalcone in refluxed ethanol and in the presence of piperidine as a catalyst, following the previously described procedure (Prasad et al., 2008). We have shown that the reaction starts by a 1,4-Michael addition to afford Michael adduct **2**, followed by a subsequent addition of a second molecule of 4-methylchalcone to afford intermediate **3**. This later undergoes intramolecular cyclization via nucleophilic addition of carbon α of the carbonyl group to the second carbonyl group to give the target cyclohexane-1,1-dicarbonitrile MPC according to the pathway proposed in scheme 1. The 4-methylchalcone used as starting material was prepared according to literature (Jacobsen, 2016).

The structure of the MPC compound (Fig. 1) was established using the usual spectroscopic techniques of IR and NMR (¹H and ¹³C). Its infrared spectrum (Fig. 2) shows several bands. The absorption band at 3412 cm⁻¹ is attributed to vibration of the O–H bond, which is complemented by the C–OH band at 1188 cm⁻¹ due to the hydroxyl groups of the carboxyl. The absorption band at 1644 cm⁻¹ is assigned to vibration of the carbonyl group (C=O). Also, the C=O band is displaced at a lower frequency by the interactions of the intramolecular hydrogen bond, which causes overlapping with the C=C band. Moreover, the C=C stretching vibrations appear at 1447 cm⁻¹ and the C–C stretching modes have been observed at 1595 and 1516 cm⁻¹. Moreover, the appearance of absorption band at 1135 cm⁻¹ corresponds to the C–N stretching mode for title compound.

In the ¹H NMR spectrum (Fig. 3), we note the presence of the following characteristic signals: two singlets at 2.16 and 2.37 ppm, corresponding to the protons of methyl groups. A doublet of doublets centered at 2.34 ppm, which corresponds to H^b. The doublet of triplets at 2.93 ppm belongs to H^c. The doublet of doublets at 4.17 ppm is attributed to the proton H^d. The protons H^e and H^f resonate as two doublets at 4.18 ppm and 4.84 ppm, respectively. The doublet at



Scheme 1 Proposed pathway for the synthesis of target cyclohexane-1,1-dicarbonitrile MPC.

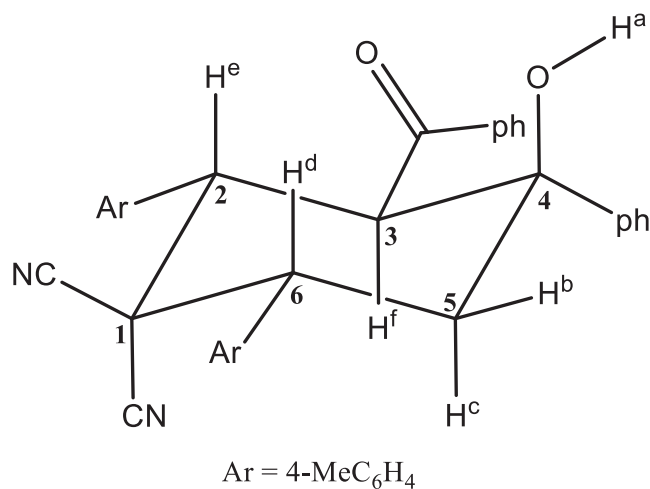


Fig. 1 Molecular structure of MPC compound.

5.16 ppm is attributed to the hydroxyl proton (OH). The ^1H NMR spectral data indicate that MPC compound adopts a chair conformation (Fig. 1), which is consistent with analogous structures described in the literature (Jacobsen, 2016).

The ^{13}C NMR spectrum (Fig. 4) of the same compound shows, in particular, the presence of a signal at 204.13 ppm corresponding to the carbon of the carbonyl group ($\text{C}=\text{O}$). The signal at 74.56 ppm corresponds to the quaternary carbon C_4 linked to the hydroxyl group ($\text{C}-\text{OH}$). The signals at 51.69, 49.84, and 45.78 ppm are assigned to C_3 , C_2 , and C_6 , respectively. The signal at 40.72 ppm is due to carbon C_5 of the methylene group (CH_2). Two other characteristic signals at 20.95 and 21.13 ppm are attributed to the carbons of methyl groups ($-\text{CH}_3$). The spectra of the MPC compound are in good agreement with the proposed structure (Fig. 1).

3.2 wt. loss (WL) measurements

3.2.1. Effect of inhibitor concentration

The WL method, which consists of measuring both inhibition efficiency and corrosion rate, is accommodated due to its ease of use and superior reliability. In this section, WL investigations are conducted in exclusion and inclusion of the inhibitor in 1 M HCl medium at 303 K to examine the effect of MPC concentrations. Data on WL for MS coupons is shown in Fig. 5, which summarizes both the inhibition efficiency ($\eta_{\text{WL}}\%$) and the corrosion rate (CR) obtained from the WL

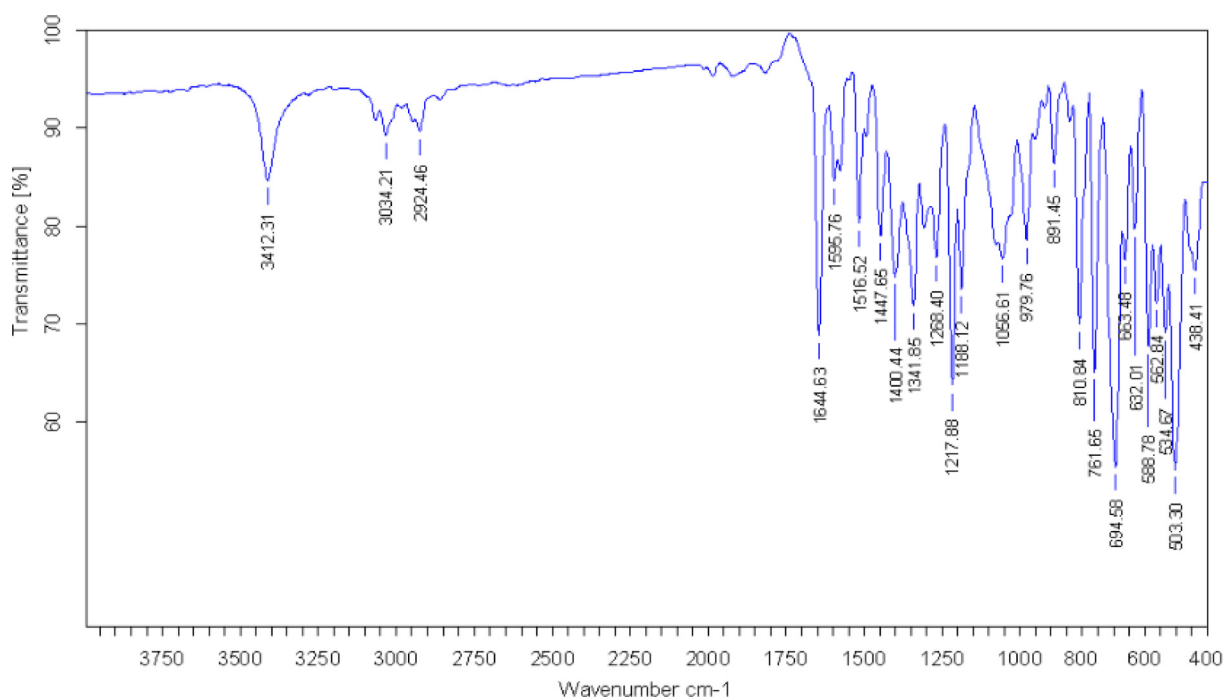


Fig. 2 Infrared spectrum of MPC compound.

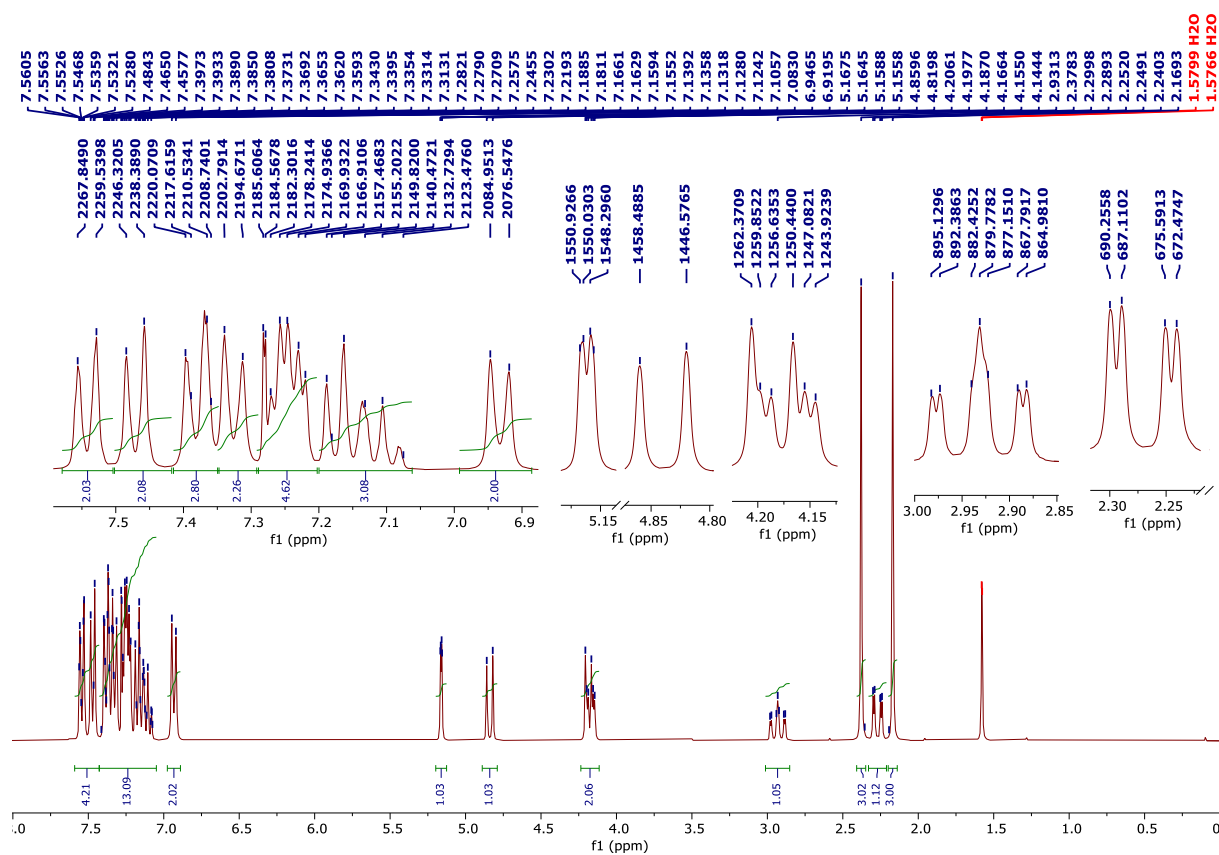


Fig. 3 ¹H NMR spectrum of MPC organic compound.

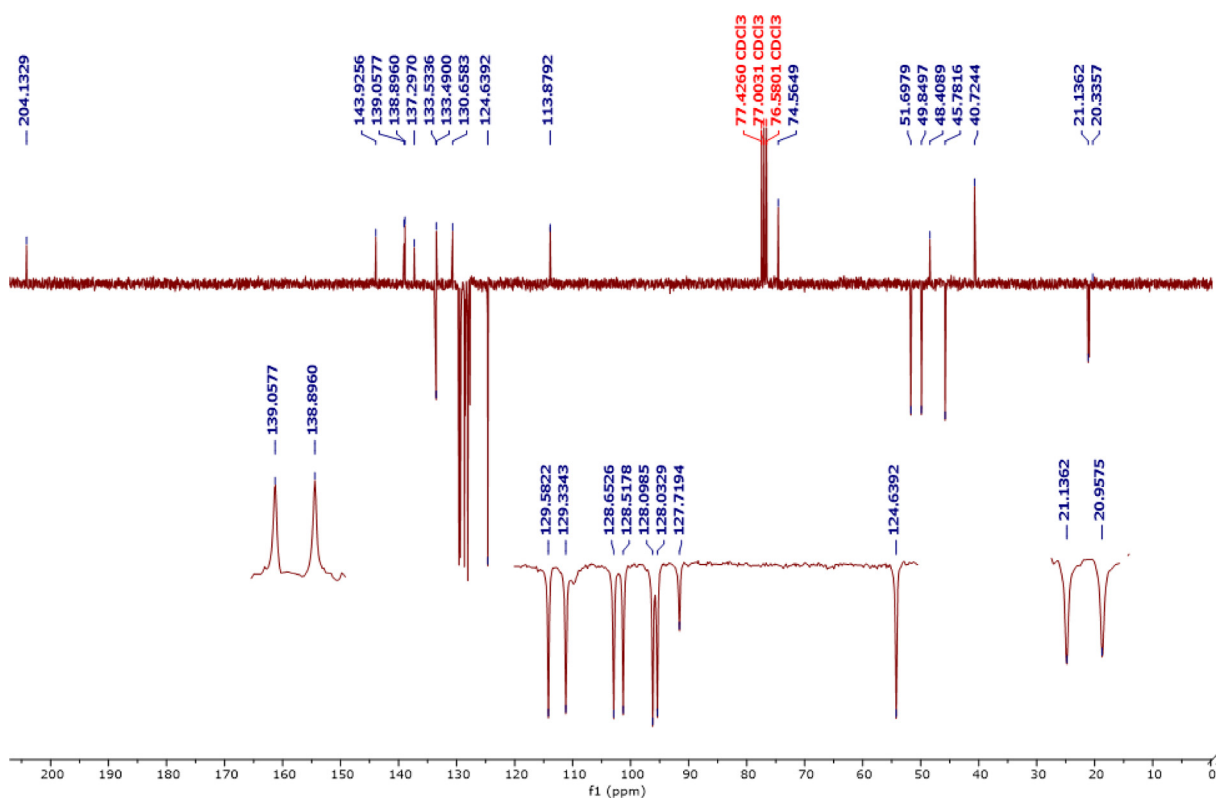


Fig. 4 ¹³C NMR spectrum of MPC organic compound.

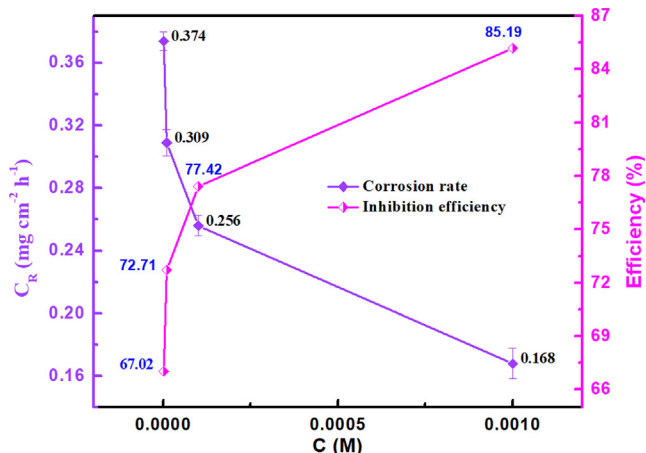


Fig. 5 Variation of C_R and inhibition efficiency with the concentration of MPC for MS in 1 M HCl at 303 K.

technique at different concentrations. Fig. 5 reveals that as the inhibitor concentration increased, the inhibition efficiency increased, demonstrating that the protective layer formed by the inhibitor on the MS surface is more compact at high concentrations owing to the adsorption of the inhibitor molecules on the metallic substrate. Also, following Fig. 5, the effect of increasing concentration on the corrosion rate values is shown. As it can be seen, the increase of the inhibitor concentration and the increase of the covering surface on the metal surface, result in a decrease of the corrosion rate values, which is probably due to the creation of a defensive layer on the metal surface and, consequently, increases its resistance against corrosion (Alamry et al., 2021; Fawzy et al., 2021; Verma et al., 2021b). According to the results, it is noticed that by increasing the concentration of the inhibitor, the adsorption is significantly improved up to the optimal value of 10^{-3} M, leading to blocking of the active sites on the surface exposed to the electrolyte (Echihi et al., 2021; Elgaddafi et al., 2021; Gaber et al., 2021). The inhibition efficiency reached 85.19 % at 10^{-3} M, indicating effective coverage of the metal substrate and high protection offered by the MPC inhibitor.

3.2.2. Effect of temperature

Temperature is an influential factor in the adsorption behavior of corrosion inhibitors in many industries that work in conditions that require high temperatures. An increase in temperature can lead to a considerable increase in the adsorption capacity, which becomes less effective by exceeding a limit, or it can even cause the decomposition of the film.

On the other hand, the rise in temperature can accelerate the rate of oxidation and reduction reactions on the metallic interface and prevent the deposition of the protective layer, which leads to the penetration of the aggressive solution on the alloy surface, consequently accelerating the corrosion rate. Also, an increase (or decrease) in temperature in corrosive environments can significantly affect the adsorption of the inhibitor molecules and can lead to the desorption of the film formed on the metallic surfaces (Iroha et al., 2021; Shaban et al., 2021). In this research study, WL tests were used to evaluate the thermal stability of the MPC compound (Table 1). Thus, the elevated temperature caused a considerable increase in the corrosion rate for the blank solution. However, the results showed that minimal

weight loss occurs at 333 K, indicating that the inhibitory efficacy of the compound is considerably stable even at high temperatures. As a whole, the investigated compound showed better resistance to the corrosion process even at high temperatures, notwithstanding the minor decrease in its inhibitory efficiency, which is related to the increase in the corrosion rate caused by a large number of effective impacts between MS and the different elements contained in the acidic medium per time unit (Mousavi and Pitchumani, 2022; Sharma and Kumar, 2021). Therefore, keeping in mind the importance of the impact parameter, the time factor is included and will be explained in the coming sections of the paper.

3.3. Overall corrosion behavior by MPC inhibitor

Using the potentiodynamic polarization method, the influence of MPC on the anodic dissolution of MS and the cathodic reduction process of hydrogen ions in 1 M HCl medium was examined. The corrosion polarization curves of the metal without and with the inhibitor in 1 M HCl are presented in Fig. 6a. The anodic and cathodic branches of the PDP curves were extrapolated to obtain the corresponding electrochemical parameters, including corrosion current densities (i_{corr}), corrosion potential (E_{corr}), cathodic Tafel slope (β_c), anodic Tafel slope (β_a), and inhibition efficiency ($\eta_{PDP}^{\%}$), listed in Table 2. The polarization curve patterns for the inhibited and uninhibited MS follow the same general shape in Fig. 6a. Hence, suggesting that the MPC inhibitor in 1 M HCl medium inhibits the corrosion of the steel through adsorption on the metal surface, blocking the active sites without disturbing the corrosion process. The MPC inhibitor only modifies the corrosion kinetics by suppressing both anodic and cathodic half-processes. At the same time, the inclusion of MPC in the acidic solution resulted in a substantial decrease in i_{corr} and an increase in $\eta_{PDP}^{\%}$, which showed reasonable agreement with the results obtained by the WL method. The implicated results reveal that as the inhibitor concentration increased, both the cathodic and anodic branches shifted to reduced current densities, i.e., a decrease in corrosion rate (Mousavi and Pitchumani, 2022). This can be well explained in Table 2 showing how the introduction of increasing doses of the compound under study produces a decrease in the corrosion current density values compared to that of the blank solution.

The presence of MPC inhibitor does not prominently shift the E_{corr} (the maximum shift in this study was < 85 mV with respect to the corrosion potential of the blank solution). This means that MPC acted as a mixed inhibitor, generating a protective layer on the metal surface. In the presence of PMC inhibitor, the slight change of both β_c and β_a confirms that the corrosion mechanism of MS does not change. These results infer that the inhibitor decreases the surface area for corrosion without affecting the mechanism of corrosion and only causes inactivation of a part of the metal surface. The corrosion parameters obtained from the PDP measurement imply that the inhibitor molecules adsorb onto the steel substrate and form a protective film, providing corrosion protection which reduces the corrosion of metal (Joseph and Joseph, 2021; Zhu et al., 2021). As a potential explanation for this behavior, it appears that there is strong coordination bonding in the active regions of the MPC involving vacant iron orbitals and heteroatoms free electrons.

Table 1 Corrosion rates (C_R) and inhibition efficiencies ($\eta_{WL}\%$) of MS corrosion in 1 M HCl solution without and with different concentrations of MPC inhibitor at different temperature.

	Solution (M)	Temperature (K)	Corr. Rate (C_R) (mg/cm ² h)	Inhibition efficiency ($\eta_{WL}\%$)
Blank	1 M HCl	303	1.135 ± 0.0121	–
		313	1.416 ± 0.0215	–
		323	1.998 ± 0.0214	–
		333	2.539 ± 0.0316	–
MPC	10⁻³	303	0.168 ± 0.0047	85.19
		313	0.262 ± 0.0090	81.43
		323	0.421 ± 0.0087	78.90
		333	0.727 ± 0.0043	71.35
	10⁻⁴	303	0.256 ± 0.0066	77.42
		313	0.383 ± 0.0052	72.94
		323	0.613 ± 0.0064	69.32
		333	0.909 ± 0.0075	64.18
	10⁻⁵	303	0.309 ± 0.0038	72.71
		313	0.439 ± 0.0029	68.98
		323	0.751 ± 0.0092	62.40
		333	1.015 ± 0.0044	60.02
10⁻⁶	303	0.374 ± 0.0065	67.02	
	313	0.512 ± 0.0089	63.81	
	323	0.780 ± 0.0043	60.94	
	333	1.054 ± 0.0077	58.48	

Additionally, the evaluation of the kinetics and mechanisms of electrochemical processes occurring at a metal/solution interface is generally carried out by the EIS method. In this case, the capacitive action of the MS electrode in the presence of various concentrations of the MPC inhibitor was studied. Nyquist and Bode plots are shown in Fig. 6b,c. A single capacitive loop is seen in both the inhibited and uninhibited metal samples, indicating that the dissolution of steel involves a single charge transfer process that takes place at the electrode/solution interface, and the presence of MPC inhibitor does not change the mechanism of dissolution of MS. Diffusion tails at low frequencies also appear in the impedance spectra of MS in 1 M HCl solution when MPC is present. The diffusion tail indicates the formation of a protective porous film on the metal surface and is related to the diffusion of soluble species from the MS surface to the bulk of the solution (mass transfer) (Chen et al., 2000).

Fig. 6b revealed that the diameters of the Nyquist plots increase with increasing inhibitor concentrations, corresponding to an increase in corrosion resistance. Furthermore, it is evident that the impedance diagrams are not perfect semicircles, which is due to the roughness and inhomogeneity of the electrode surface, which contribute to frequency dispersion (Li et al., 2010). The electrical equivalent circuit used to fit the impedance data are depicted in Fig. 6d, for blank and inhibited solutions. To get a more precise and optimum fit, double layer capacitance (C_{dl}) in the circuit was converted to a constant phase element CPE_{dl} (Q_{dl} , n) in the equivalent circuit. However, C_{dl} values are estimated by applying the following relation (Chugh et al., 2020):

$$C_{dl} = \sqrt[n]{Q_{dl} \times R_p^{1-n}} \quad (8)$$

where Q_{dl} and n are the major components of CPE_{dl} . Value of n is always between 0 and 1 as it justifies the difference from an ideal behavior. The parameter of n quantifies different

physical phenomena like surface inhomogeneousness resulting from surface roughness, inhibitor adsorption, porous layer formation, etc.

Table 3 lists the results of the fitting procedure for inhibition efficiencies and other impedance parameters. The proposed circuit's validity was further corroborated by the goodness of fit values (χ^2), which were of the order of 10^{-3} , as well as by the coherence of the experimental data (points) and fitted curves (solid line) displayed in the Nyquist plots. From the quantitative results shown in Table 3, it appears that the introduction of the MPC inhibitor into MS inhibits corrosion. As the MPC concentration increases, polarization resistance (R_p) increases, but C_{dl} decreases. This behavior is due to the formation of a protective film of MPC inhibitor on the MS surface, and the film quality is improved with the increase in inhibitor concentration. Additionally, the variation in the n -values can also be attributed to the adsorption of inhibitor molecules and the formation of porous layers (Zhong et al., 2021). The inhibition efficiency ($\eta_{EIS}\%$) improves with increasing inhibitor concentration and the maximum $\eta_{EIS}\%$ reaches 85.63 %, which further confirms that MPC acts as an exceptional inhibitor. The inhibition efficiencies calculated from EIS are in good agreement with those obtained from PDP and WL measurements.

Bode diagram representation of the EIS (Fig. 6c) reveals that the impedance modulus is continually increasing with increasing inhibitor concentration. The maximum impedance can be observed in the low frequency region, suggesting the formation of a film of inhibitor molecules on the metal surface (Golabadi et al., 2021). As well, the phase angle plots show a concomitant increase in phase angle with increasing inhibitor dose in acidic solution, indicating an improvement in the capacitive performance of the metal/solution interface. These results suggest that the adsorption of the inhibitor leads to a protective film that mitigates the corrosion. The non-ideal

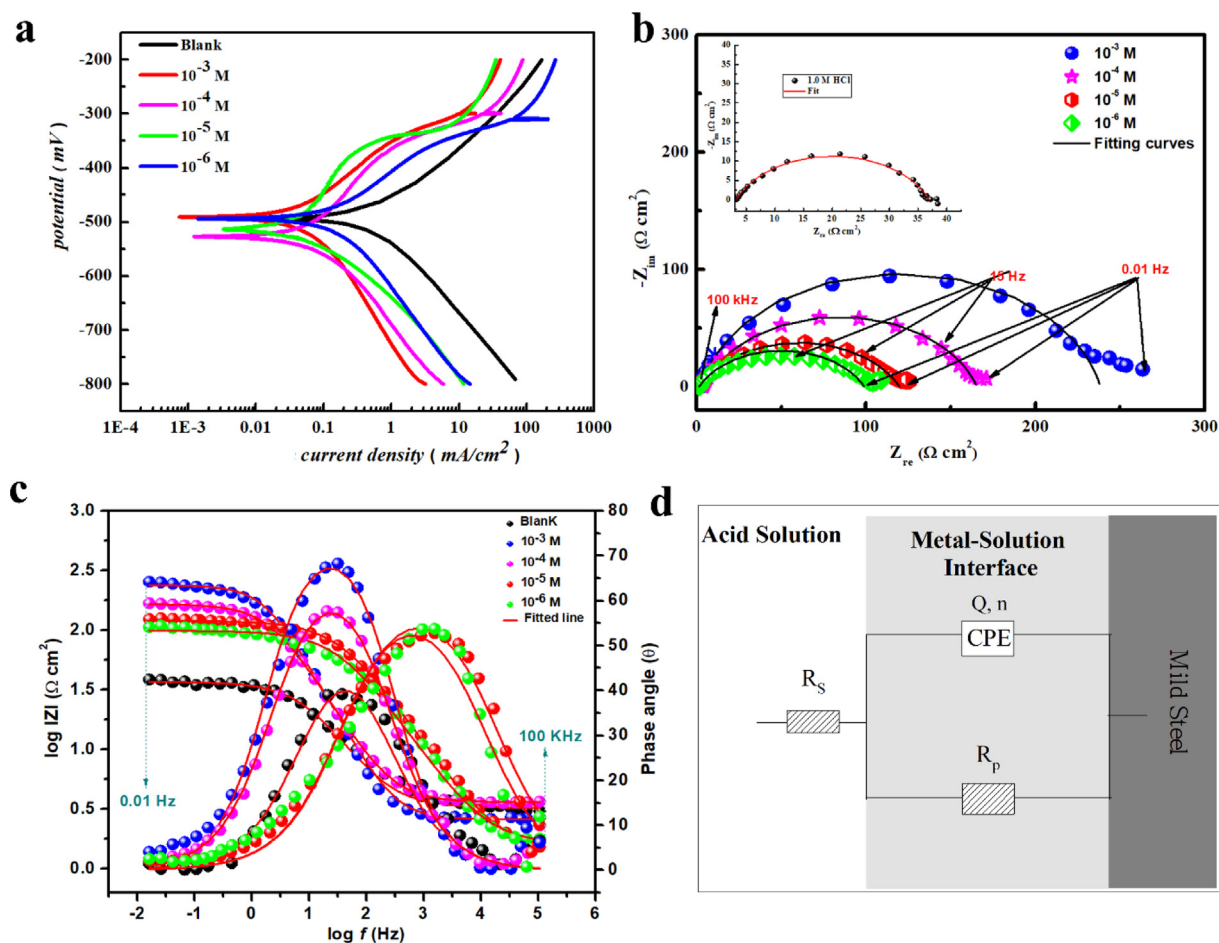


Fig. 6 (a) PDP curves, (b) Nyquist plots, (c) Bode impedance modulus and phase angle plots for MS in inhibited and uninhibited 1 M HCl solution to evaluate the overall corrosion behavior, and (d) equivalent circuit models used to fit the experimental impedance data.

Table 2 PDP results for MS corrosion in 1 M HCl solution without and with different concentrations of the MPC inhibitor.

	Concentration (M)	$-E_{\text{corr}}$ (mV vs SCE)	$-\beta_c$ (mV dec $^{-1}$)	β_a (mV dec $^{-1}$)	Corr. Rate (mm/year)	i_{corr} ($\mu\text{A cm}^{-2}$)	η_{PDP} (%)
Blank	1.0	490.10	140.13	101.20	6150	521.02	–
MPC	10^{-3}	493.90	168.03	105.40	864	73.90	85.81
	10^{-4}	529.80	139.51	76.90	1269	108.5	79.17
	10^{-5}	516.10	141.90	94.30	1642	140.50	73.03
	10^{-6}	496.53	112.40	118.90	2066	176.70	66.08

behavior of the electrochemical system is supported by the phase angles' deviation from the 90° ideal capacitive value.

3.4. Long term immersion and adsorption isotherm model

For a complete overview of the parameters impacting the adsorption phenomenon and its subsequent dependence on the organic compounds' efficiency, the present work section highlights the effect of immersion time among the most important factors influencing the inhibition performance, after having studied the effects of concentration and temperature on inhibition in preceding sections. The findings of this investigation are summarized in Table 4.

Nyquist plots of MS in 1 M HCl without and with the optimum concentration of 10^{-3} M MPC at 30 min, 24 h, 48 h and 72 h are shown in Fig. 7a,b. It clear from the Fig. 7a,b that R_p is time dependent. The semicircles diameters are decreasing following the successive increase of the immersion times in the uninhibited (Fig. 7a) and inhibited (Fig. 7b) solutions. Based on the observed data, the R_p values decrease with increasing immersion time. For uninhibited solutions, the protective film (i.e., corrosion products) is not protective enough, so it promotes the charge transfer of electrons with immersion time. In inhibited solutions, the semicircular loops and therefore R_p values obtained at all immersion times studied are larger than those in the case of uninhibited solutions, suggesting that

Table 3 Impedance parameters for MS corrosion in 1 M HCl solution without and with different concentrations of the MPC inhibitor.

	Concentration (M)	$R_p (\Omega cm^2)$	n	$Q \times 10^{-4} (S^a \Omega^{-1} cm^{-2})$	$C_{dl} (\mu F cm^{-2})$	Goodness of fit (χ^2) $\times 10^{-3}$	η_{EIS} (%)
Blank	1	33.69	0.87	1.8820	88.34	1.23	–
MPC	10^{-3}	234.60	0.84	0.3715	15.05	2.59	85.63
	10^{-4}	161.90	0.80	0.6824	22.12	3.60	79.19
	10^{-5}	118.50	0.81	0.8253	27.87	2.41	71.56
	10^{-6}	97.32	0.82	0.9520	34.06	2.58	65.38

Table 4 Long-term electrochemical impedance parameters of the MS surface in inhibited and uninhibited 1 M HCl solution.

	Time (h)	$R_p (\Omega cm^2)$	n	$Q \times 10^{-4} (S^a \Omega^{-1} cm^{-2})$	$C_{dl} (\mu F cm^2)$	Goodness of fit (χ^2) $\times 10^{-3}$	η_{EIS} (%)
Blank	0.5	33.69	0.87	1.8820	88.34	1.23	–
	24	28.88	0.88	2.0983	104.63	3.13	–
	48	21.88	0.86	2.7723	120.75	3.34	–
	72	18.42	0.84	3.8653	150.70	3.37	–
MPC	0.5	234.60	0.84	0.3715	15.05	2.59	85.63
	24	188.40	0.81	0.5691	19.64	3.62	84.67
	48	134.30	0.83	0.6934	26.60	3.87	83.70
	72	108.79	0.82	0.8962	32.43	3.16	83.06

the blocking of the dominant corrosive sites of the metal by adsorption of MPC molecules on the metal is mainly regulated by the charge transfer process (Guo et al., 2021).

However, when more inhibitor molecules are adsorbed on the steel surface, the inhibitor adsorption density increases to a suitable level, allowing van der Waals force to interact between inhibitor molecules. As a result, it is anticipated that some inhibitor molecules will leave the surface, resulting in a reduction in the effective area that the inhibitor covers and, consequently, a reduction in η_{EIS} % (Mobin et al., 2016). Additionally, after 72 h of exposure, the inhibitive efficacy of MPC molecules was maintained to 83.06 %, indicating that MPC was a long-range effective inhibitor for MS in a 1 M HCl environment. The stability of performance, which shows up in the best inhibitory efficiencies during different immersion times, is especially attributed to the strong adsorption of our compound with the metal surface. This high strength is achieved by connecting the hetero-atoms and aromatic ring free electrons to the empty d-orbital of iron atoms (Beniken et al., 2022; Zaidon et al., 2021).

Furthermore, several isotherm models can explain the electrochemical behavior and may be used to decouple the different electrochemical processes at the metal-solution interface according to the nature of the physical and chemical processes of the electrochemical system under investigation. Thus, the protecting ability of a chemical inhibitor against corrosion can be understood by employing a suitable adsorption isotherm. The study was carried out to examine MPC-metal adsorption. The findings concluded that the adsorption of inhibitor on the metallic surfaces follows the Langmuir adsorption model, with slope and regression coefficient approaching unity at all temperatures studied (Fig. 7c), which is given by equation (Zhang et al., 2022):

$$\frac{\theta}{1-\theta} = K \times C \leftrightarrow \frac{C}{\theta} = \frac{1}{K_{ads}} + C \quad (9)$$

Where C is for the concentration of the MPC compound, the constant of adsorption equilibrium is shortened to K_{ads} , and surface coverage is θ . The K_{ads} values were calculated from the intercepts of the straight lines and correlated to the standard free energy of adsorption (ΔG_{ads}^o) using the following equation (Zhang et al., 2022):

$$K_{ads} = \frac{1}{55.5} \times \exp\left(-\frac{\Delta G_{ads}^o}{RT}\right) \quad (10)$$

Thermodynamically, ΔG_{ads}^o is related to the enthalpy (ΔH_{ads}^o) and entropy (ΔS_{ads}^o) of adsorption process respectively, by equation (Zhang et al., 2022):

$$\Delta G_{ads}^o = \Delta H_{ads}^o - T\Delta S_{ads}^o \quad (11)$$

Fig. 7d shows the plot of ΔG_{ads}^o versus T which gives a straight line with an intercept of ΔH_{ads}^o and a slope of $-\Delta S_{ads}^o$. The ΔG_{ads}^o values indicate a predominant mode of chemical adsorption. The negative sign is indicative of the spontaneity of the adsorption process. The significant K_{ads} values indicate that inhibitor molecules and metal surfaces have strong interactions. The negative value of ΔH_{ads}^o ($-8.75 \text{ kJ mol}^{-1}$) indicates that heat is released during the adsorption process (exothermic process). Exothermic adsorption processes often signify either physisorption or chemisorption, whereas endothermic processes are unmistakably linked to chemisorption (Martinez and Stern, 2002). The positive ΔS_{ads}^o values (average value $106.23 \text{ J mol}^{-1}\text{K}^{-1}$) mean that the entropy of the adsorption process increases and this supports the adsorption of MPC molecules and the desorption of H_2O molecules (Wang et al., 2021). Some relevant information

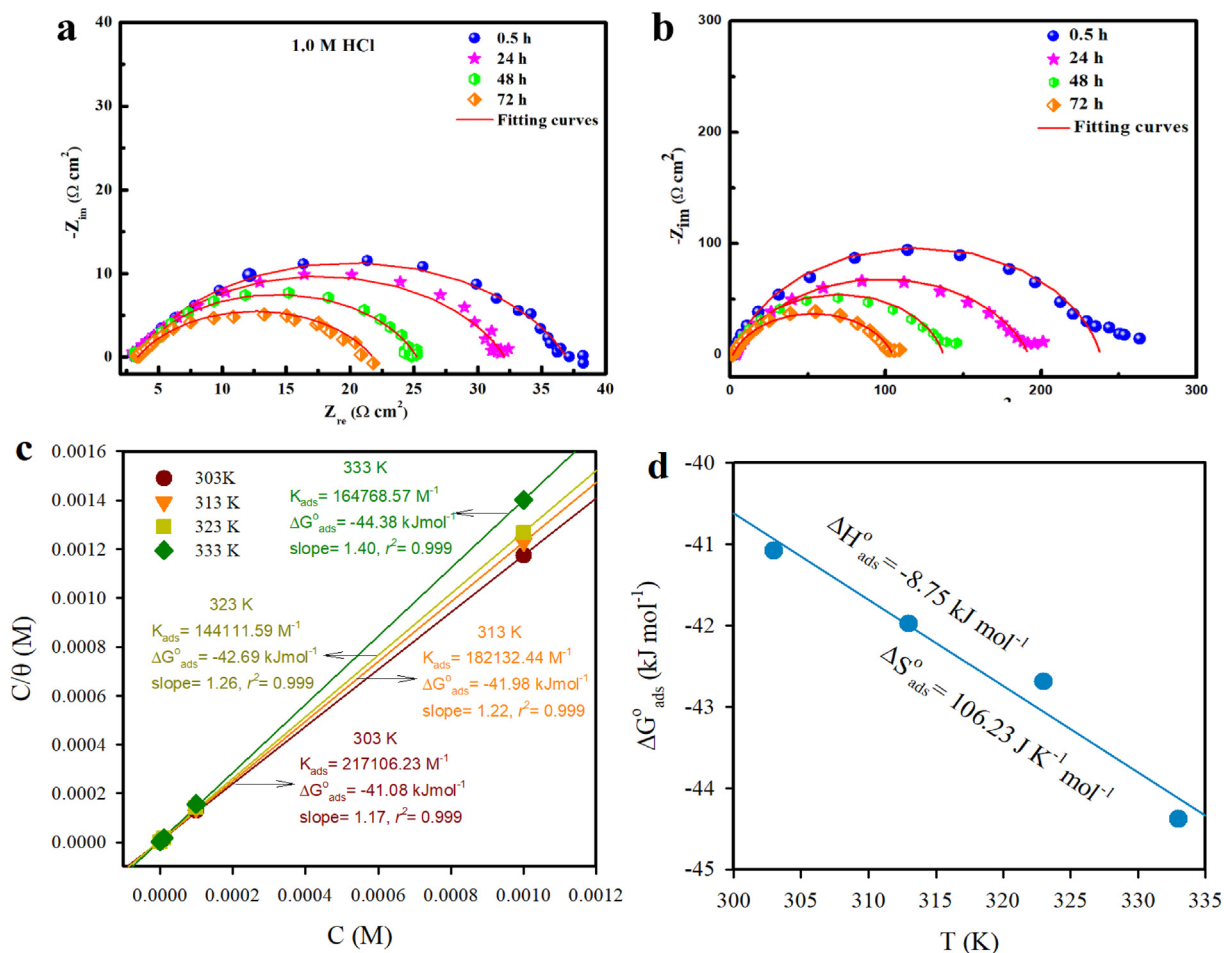


Fig. 7 Electrochemical impedance responses of the MS surface, presented in the Nyquist plot for long-term immersion (a) free solution (b) with MPC inhibitor (c) Langmuir isotherm model suitable for the adsorption of MPC and (d) the variation of ΔG_{ads}° with T .

about the adsorption process of the inhibitor can be obtained by comparing activation energy (E_a) values in both the absence and presence of the corrosion inhibitor by using the Arrhenius equation. The blank solution has a lower activation energy ($23.08 \text{ kJ mol}^{-1}$) than the inhibited solutions ($29.55 \text{ kJ mol}^{-1}$ at 10^{-6} M and $40.81 \text{ kJ mol}^{-1}$ at 10^{-3} M), indicating a strong inhibitive action of PMC inhibitor by increasing the energy barrier for the corrosion process (Quraishi et al., 2021).

3.5. Surface morphology studies

In the presence and absence of MPC, SEM was used to analyze the surface morphology of metals after 72 h of immersion in 1 M HCl. The resultant micro-images are given in Fig. 8. According to the images, the metal surface is strongly corroded in 1 M HCl solution (Fig. 8a), as evidenced by the rough, cracked, and damaged surface. In contrast, the corrosion process in the presence of MPC is effectively inhibited. The MPC inhibitor forms a very adherent and homogeneous inhibitor layer on the steel surface, thus reducing the corrosion of the metal (Fig. 8b). The influence of the MPC on the surface behavior of the steel is illustrated by the surface morphology

study, which supports the results obtained from the electrochemical data. The elemental composition of mild steel is determined using EDS before and after its surface is immersed for 72 h (Fig. 8c,d). Moreover, some differences were determined in the elemental analyses of the resultant organic layer in which the N element was detected, and the C peak contribution increased as a result of the carbon atoms of the MPC compound. In addition, the apparition of C and N elements was attributed to the polar functional groups as well as the aromatic structure of the organic compound. Thus, the addition of MPC organic inhibitor to the corrosion test solution clearly contributed to a significant change in the surface morphology of the metal surface and new structure may provide corrosion protection for the entire surface. These results supplement and confirm the findings of the WL, EIS, and PDP tests and further explain the high adsorption performance of MPC inhibitor.

3.6. Multi-level computational perspectives

3.6.1. Electron donor–acceptor behavior of MPC molecule

To clarify the corrosion inhibition mechanism which was activated by the addition of MPC inhibitor, quantum chemical (QC) calculations were performed using several computational

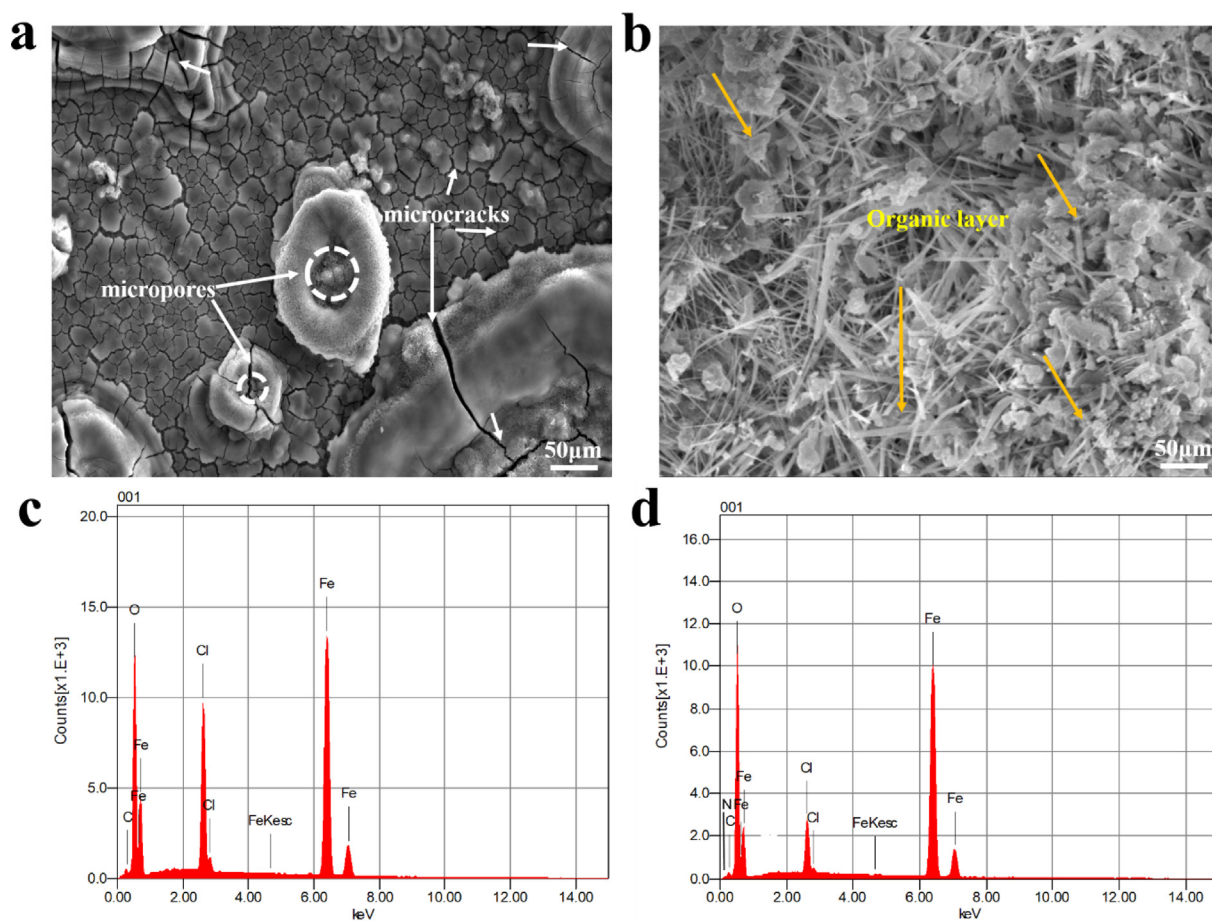


Fig. 8 Morphologies of MS surface after long-term corrosion test in (a) uninhibited, and (b) inhibited 1 M HCl solution and (c,d) their elemental composition.

functions (Guo et al., 2017; Luo et al., n.d.). Molecular orbitals (MO) are single-particle wave functions formed by the linear combination of atomic orbitals and are also crucial parameters for measuring molecular properties and electron transfer in molecules. In terms of density flooding theory, QC descriptors are significant in predicting the active and adsorption centers of organic corrosion inhibitors. Thus, in the present work, QC calculations were calculated to evaluate the inhibition effect in relation to electron transfer behavior between organic film and steel surface. The density distribution of the frontier MO of MPC inhibitor is shown in Fig. 9a,b. The obtained QC parameters such as E_{HOMO} , E_{LUMO} , ΔE , χ , and ΔN , and other parameters are listed in Table 5. Based on Fig. 9a,b, the MO population is distributed around aromatic and different donor-acceptor sites. The whole region of the planar structure is the active center, with several feasible adsorption sites adsorbed on the surface of the metal. Additionally, HOMO and LUMO energies are mainly related to the electron-donating and electron-accepting ability of an inhibitor molecule. It is known that low E_{LUMO} demonstrates the ability of the molecule as an electron-acceptor, whereas a tendency of the organic molecule to donate electrons to the suitable acceptor can be inferred by the high value of E_{HOMO} (Musa et al., 2012). However, the separation energy (ΔE) describes the stability of a molecule. A low value of ΔE indicates that a molecule would potentially be adsorbed more easily on the metallic

surface. It is clear that the reactivity of MPC towards the steel substrate increases, thus leading to an enhanced adsorption performance of the molecule. From the energetic position of MO, the E_{HOMO} of MPC (-6.77 eV) is much nearer to Fermi level of Fe (-5.17 eV) than E_{LUMO} (-2.19 eV). Moreover, the energy difference between E_{HOMO} of MPC and the Fermi level of iron is very low (-1.60 eV), which reflects the charge transfer behavior of MPC molecules (Fig. 9c). Furthermore, the ΔN value was correlated to the adsorption performance resulting from electron donation, in which the bonding efficiency is assessed by the fraction of π - and free-electrons transfers from the MPC inhibitor to the metallic surface. If $\Delta N < 3.6$, the adsorption performance would be improved by either an increase in HOMO energy or a decrease in separation energy.

However, the possibility of evaluating the bonding efficiency based only on the QC parameters of the isolated molecules must be thoroughly investigated because some QC parameters may not always be reliable for clarifying reactivity and describing electron transfer behavior of the molecule. Therefore, the evaluation of charge transfer behavior from other DFT perspectives is necessary. Thus, total density of states (TDOS), electron localization function (ELF) and electrostatic potential (ESP) distribution on the van der Waals (vdW) surface are useful functions in characterization of lone pair electrons and they have a close relationship with molecular properties that are related to lone pairs and localized MO

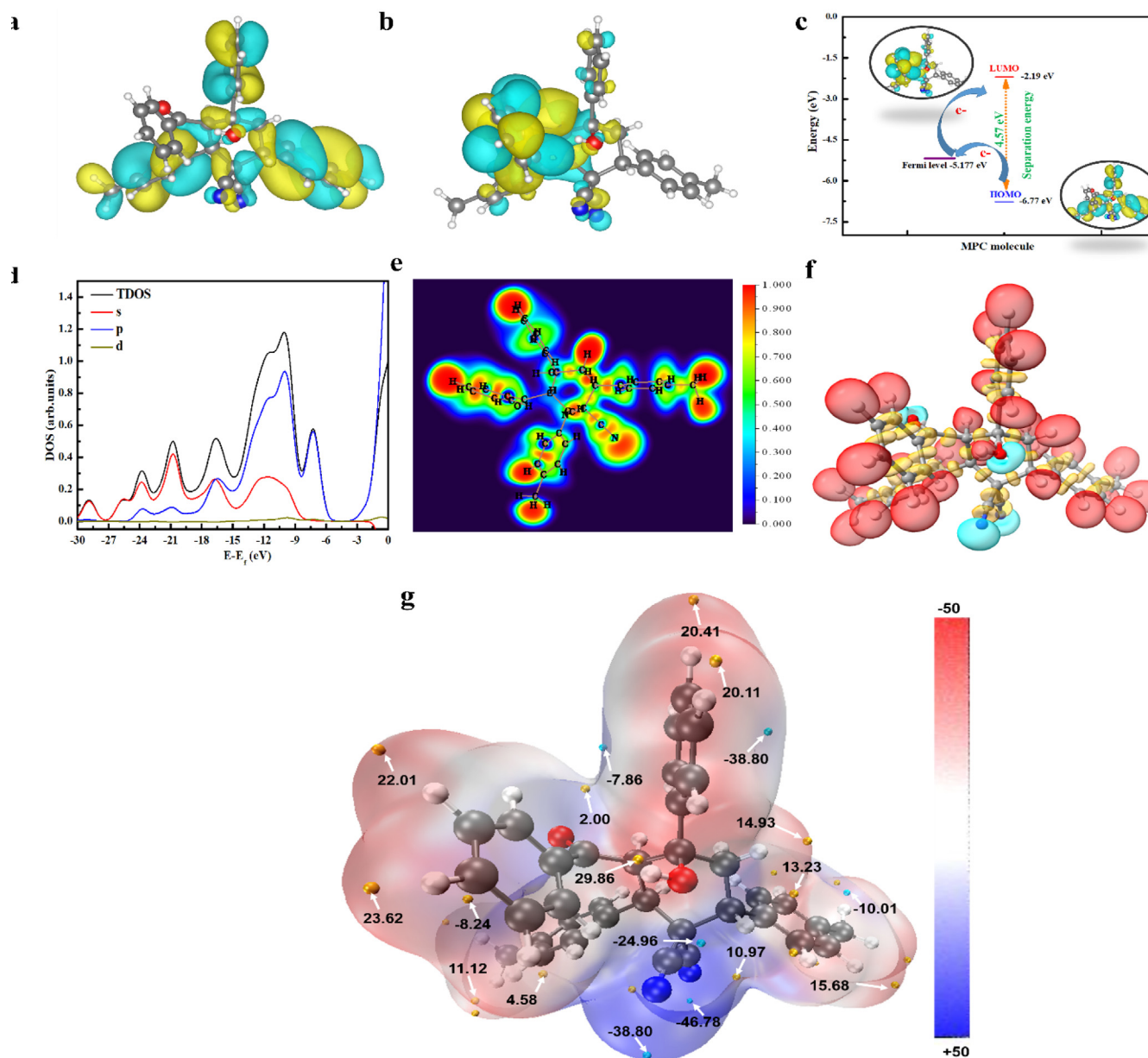


Fig. 9 (a) HOMO, (b) LUMO, (c) energetic positions, (d) density of states of frontier orbitals, (e) ELF color-filled maps in the XY plane, (f) ELF isosurfaces (color code: cyan for lone pair domains, red for hydrogen-related domains and yellow for bonding domains between heavy atoms; isosurface 0.796 a.u.), and (g) ESP mapped vdW surface (color code: orange and blue spheres correspond to ESP maxima and minima on the vdW surface, respectively; isosurface 0.001 a.u.).

Table 5 Molecular reactivity of MPC molecule described from quantum chemical descriptors using DFT-molecular simulation.

Parameters → Molecule ↓	E_{HOMO} (eV)	E_{LUMO} (eV)	IP (eV)	EA (eV)	ΔE_{gap} (eV)	χ (eV)	ω^+	ω^-	ΔN_{110}
<i>DFT Calculations at B3LYP/6-311G++(d,p) level</i>									
MPC	-6.77	-2.19	6.77	2.19	4.57	4.48	2.42	6.90	0.03

(Chaouiki et al., 2022a; Jiao et al., 2021). The TDOS was simulated based on the distribution of MO energy levels. The TDOS and the contribution of each orbital in electron transfer

behavior are depicted in Fig. 9d. It can be inferred that the occupied MO are mostly contributed by s and p orbitals, which is due to the important role of the electron-rich regions

of MPC. Furthermore, the ELF isosurface and the color-filled map (along the XY plan) provide useful insights into donor–acceptor interactions, and the results confirm the importance of aromatic ring π -electrons as well as the remarkable contribution of O–H and C \equiv N groups to succinct electron transfer (Fig. 9e,f). Thus, it is primordial to predict the electron transfer behavior of MPC molecules based on their interfacial interactions, particularly hydrogen bonds with hydroxyl groups and lone pair electrons.

In order to predict the intermolecular interactions and determine the nucleophilic and electrophilic sites of the MPC molecule, the ESP colored vdW surface along with surface extrema were provided. The more negative (red region) and more positive (blue region) ESP sites are indicative of electrophilic and nucleophilic sites, while orange and blue spheres correspond to ESP maxima and minima on the vdW surface, respectively. A closer inspection of Fig. 9f reveals that the most negative potential (global surface minimum) was located at the one N-atom of C \equiv N group with an ESP value of -46.78 kcal mol $^{-1}$, whereas the ESP distribution around the H atom in the O–H group is the global surface maximum, which corresponds to the most positive values. These results suggest that the lone pair of electrons on the O and N atoms may act as nucleophilic reaction sites during the interaction between the MPC inhibitor and the vacant orbital of Fe. Thus, it is believed that the presence of hydroxyl group increases the chemical reactivity and adsorption potential of MPC, indicating the stability and large polarity toward strong coordination bonds and the formation of an adhesive organic layer on the metallic surface.

3.6.2. Adsorption of MPC inhibitor

On the basis of DFT-molecular simulation, we assumed the electron transfer behavior in the MPC structure clearly influenced its reactivity. In fact, by analyzing several reports and the structures of large inhibitor molecules, the parallel configurations of these adsorption systems were studied using a relatively simple method, i.e., DFTB (Guo et al., 2017). Two

parallel configurations of the MPC molecule were studied on the iron surface to describe the intermolecular interactions occurring between chosen models and Fe(110). Accordingly, the most stable adsorption configurations of the MPC molecule on the iron surface are shown in Fig. 10. In addition, the adsorption energy is calculated, and the results are summarized in each orientation. In the first model, the MPC molecule is located on the Fe(110) surface, where the two N-atoms of C \equiv N groups are in direct chemisorption interaction with the Fe(110) surface (Fig. 10a). On the contrary, in the second model, the MPC molecule interacts with iron surface through the O atom of the hydroxyl group, as shown in Fig. 10b. Interestingly, the MPC molecule interacts with the Fe surface in a nearly flat arrangement and the π -current of the phenyl rings is in direct interaction with the Fe surface, suggesting that the electron transfer takes place between the adsorbed MPC inhibitor and the Fe(110).

In addition, the MPC...Fe bond distances are 1.78 and 2.20 Å, measured from the N and O atoms to the adjacent Fe atoms, respectively. In fact, chemical bond formation was favored in both adsorption geometries because the covalent radii of the bonded atoms (N, O) and Fe are within the sum of the covalent radii of N, Fe atoms ($r_N + r_{Fe} = 2.07$ Å), and O, Fe atoms ($r_O + r_{Fe} = 1.98$ Å) (Zhang et al., 2017). These findings clearly show that the adsorbed MPC has strong intermolecular and covalent interactions with the Fe(110) surface, which are primarily formed by electron transitions from the inhibitor to the Fe 3d band state. In the Fe(110) adsorbed parallel (N contact) system, it is remarkable that MPC exhibits high adsorption energy (-5.83 eV) compared with that of the second system (O contact, -4.98 eV). This suggests that the adsorption of MPC molecules is presumably affected by the electron-donating groups in conjunction with the reactive sites, which leads to strong bonding and superior stability of self-assembly formed on the Fe surface. The above results showed that the robust interaction between C \equiv N groups and the iron surface might be the key driving factor for the adsorption and charge transfer behavior on the Fe(110) surface.

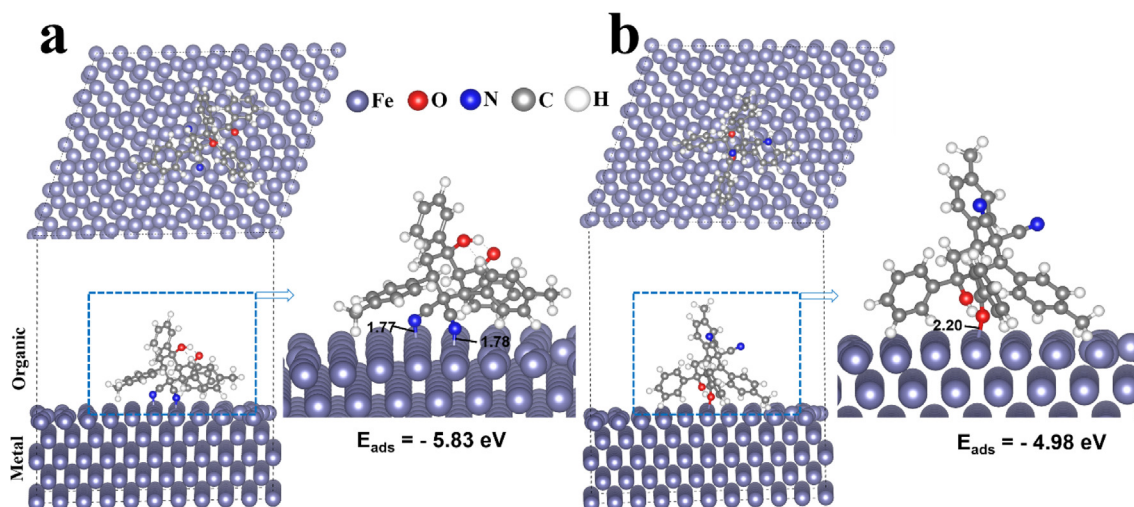


Fig. 10 Computational perspectives on the adsorption behavior of MPC on the Fe surface. Configuration of the MPC molecule adsorbed on the Fe (110) surface from the side and top view simulated using DFTB concept. (a) C \equiv N contact and (b) O–H contact together with the corresponding adsorption energy.

3.6.3. MD simulation results of MPC/Fe interactions

According to the DFTB results, the strong resonance-stabilized structure of MPC led to an increase in the stability and electron transfer behavior, which makes it easier to interact and adsorb on the Fe(110) surface. At the molecular scale, the dynamic behavior and MPC interactions with metal substrate in the presence of corrosive species were evaluated using MD simulations. Furthermore, a more thorough explanation of the interactions that will lead to a closer understanding of the mechanism in action has been obtained by the visualization of the correlative adsorption behavior. To this end, two MPC molecules and a corrosive solute were considered as an intermediate layer to simulate the interfacial mechanism of the MPC inhibitors. Fig. 11a,b shows the initial and final superstructure model of the neutral and protonated MPC on the Fe surface. A closer inspection of Fig. 11b indicates that both neutral and protonated states of MPC inhibitor tend to move towards the Fe surface, where the π -current of the aromatic rings and C \equiv N groups directly interact with the Fe surface. Interestingly, molecules in the initial adsorption system are fairly distant from the Fe surface and there are predominantly interactions between MPC-MPC, which can be considered as the primary formation of self-assembly layers. In addition,

the interaction between MPC molecules facilitates charge transfer and overlap between donor sites and the Fe surface, which can contribute to intermolecular bonding interactions. Similar to neutral MPC, the protonated state of inhibitor is preferentially oriented and tilted with its phenyl rings parallel to the metal surface with the same alignment.

Moreover, the adsorption energy is an important factor in evaluating the adsorption behavior of inhibitor molecules for each configuration. The high adsorption energy value indicates easy adsorption of both neutral and mono-protonated inhibiting species on the Fe surface, which leads to mutual and strong interactions (Haris et al., 2020). As a result, MD simulations demonstrated that the adsorption behavior of MPC molecules is in accordance with the inductive effects of functional groups and reactive sites of MPC that are adsorbed on the substrate surface in a nearly horizontal orientation, describing their optimal interactions with the Fe surface. In the presence of insulated pairs on each of the nitrogen and oxygen atoms, the molecule is rendered much more polarized to facilitate the transfer of electrons onto the metallic surface (Ebenso et al., 2021). Moreover, E_{ads} value of MPC is slightly lower than $[\text{MPCH}]^+$ which can be attributed the additional electron-donating OH group in $[\text{MPCH}]^+$. Finally, a reasonable corre-

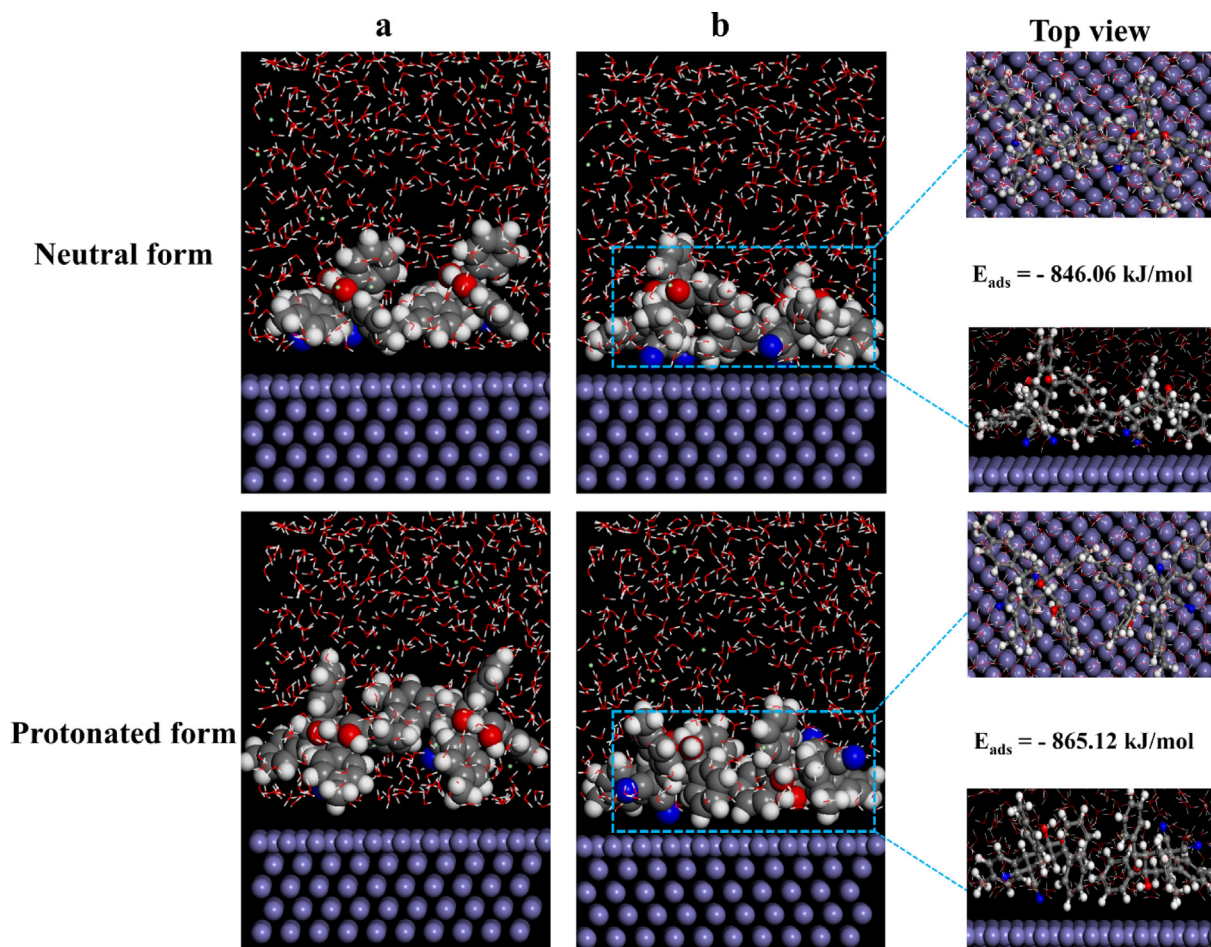


Fig. 11 Most stable patterns of neutral and protonated MPC inhibitor on Fe (110). (a) The initial and (b) final adsorption geometries in the presence of corrosive species using MD simulations (high symmetry configurations for two organic molecules).

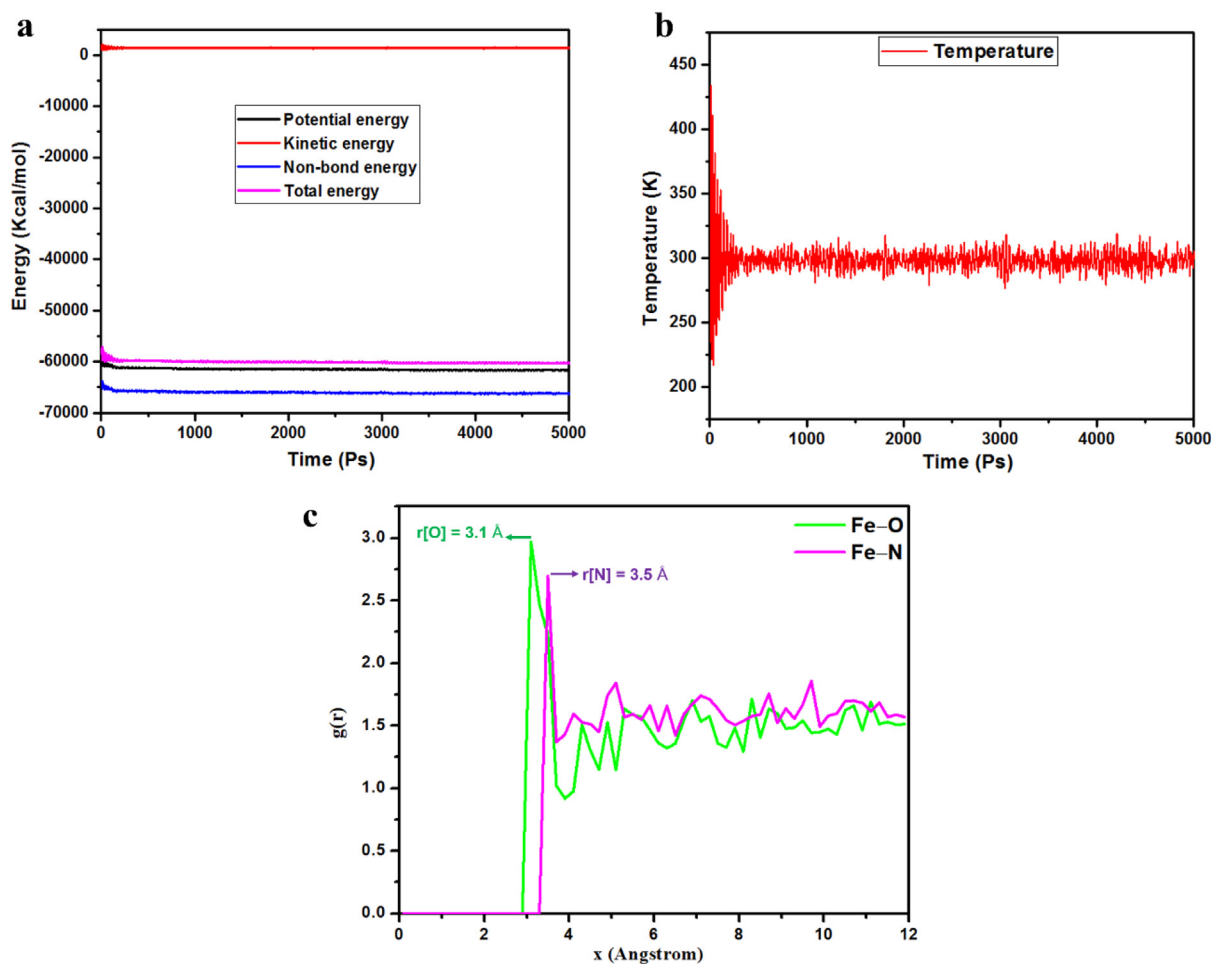


Fig. 12 (a) Energy equilibrium and (b) Temperature fluctuation curves of the MPC-Fe system during the MD run in the simulated corrosion solution. (c) Intermolecular interactions between O and N atoms in MPC molecule and Fe surface gained via RDF analysis.

spondence between the QC calculations, DFTB and MD simulations was obtained, in which we can confirm that the horizontal orientation of the MPC molecule on the iron surface minimizes the contact area between the corrosive elements and the Fe surface and forms a compact barrier that protects the metal surface. This fact might render the anti-corrosive mechanism of MPC molecules as organic inhibitors for Fe surface thermodynamically favorable, due to the adsorption of MPC molecules on the Fe surface.

From MD results, it can be inferred that the organic molecule, i.e., MPC, is an appropriate linker for the formation of well-organized protective organic layer on active surface, due to its ability to serve as a donor and acceptor of electron, in addition to its π -conjugated molecular structure. To verify the equilibrium state for all studied systems, the energy and temperature fluctuation curves were provided, as shown in Fig. 12a,b. The results confirm that the equilibrium state for studied systems is maintained in most of the time (5000 steps). Moreover, by analyzing the structure of MPC molecule, Radial Distribution Function (RDF) was completed to elucidate the strong mutual interaction between MPC and iron surface, deepening our theoretical understanding of the strongly bound and covalent organic-inorganic interfaces. The first noticeable peak in the RDF curves can be used to determine

the interaction mode of the MPC molecule on the iron surface using RDF simulated from MD trajectories. What is notable in the RDF results is that the reactive centers in the MPC molecule, i.e. the O and N atoms, have their first pronounced peaks (indicating bond lengths) at 3.1 and 3.5 Å, respectively. This finding demonstrates the synergistic contribution of π -electrons and heteroatoms of MPC to boosting the adsorption ability on the Fe surface. Interestingly, MPC inhibitor adsorbed parallel to the iron surface via O and N atoms and consistent with an improved chemical interaction, i.e. during adsorption process, there is chemisorption interaction between the O and N atoms in the MPC molecule and the Fe atoms of the iron surface. These results are highlight the bond lengths of Fe-O and Fe-N distances which are between 1 and 3.5 Å (Chaouiki et al., 2022b).

3.7. Corrosion inhibition mechanism

In view of the experimental and theoretical findings and their discussed results, the schematic of a plausible mechanism of corrosion and inhibition of the steel surface in the presence of MPC inhibitor is illustrated in Fig. 13. For the general direction of the inhibitor-steel exchange, an adsorption mechanism will be used. In the first place, a neutral form of the inhi-

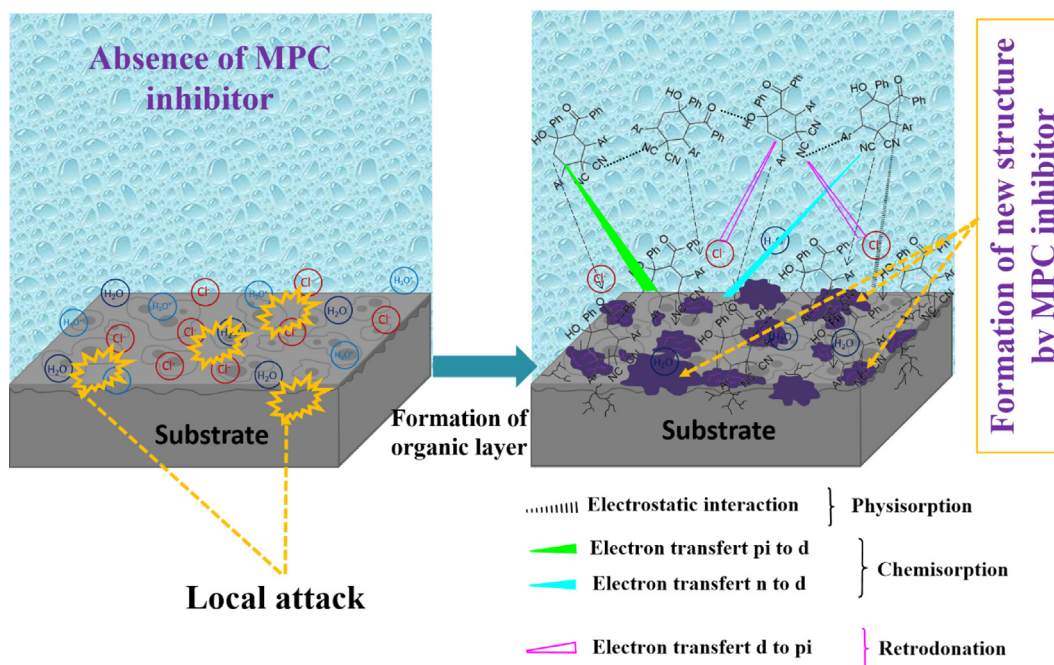


Fig. 13 The anti-corrosive mechanism schematic of MPC inhibitor molecule on the surface of Fe proposed in the present study. A growth of new structure is associated with the corrosion reaction causing the formation of coordination complexing compound between MPC inhibitor and corrosive solution.

inhibitor compounds can be adsorbed on the iron surface by chemical bonding (chemisorption), which causes displacement of H_2O molecules from the MS surface and sharing of electrons between O and N and the iron surface. This is confirmed by the adsorption energy value, which gives an idea of the corrosion inhibition of the molecule under study. This means the possibility of a constant adsorption of the MPC on the iron surface, replacing the water molecules, thus protecting the iron from aqueous corrosion. Besides, the aromatic rings include phenyl and 4-methylphenyl play a key role in the donor–acceptor exchange process that interacts with the d-orbital of the iron atom using π -electrons. Considerably, electrostatic repulsion prevents the protonated inhibitor from interacting smoothly with a positively charged steel surface (Banerjee and Malhotra, 1992; Lebrini et al., 2005; Noor and Al-Moubaraki, 2008). Accordingly, accumulated Cl^- ions on the MS surface transform its interfacial charge.

In addition, a second type of adsorption takes place for molecules that have undergone protonation. In this case, we speak of another mode of adsorption, which is physisorption. So, via electrostatic interactions set up between the positive charge of the protonated molecule and the negative charge of the Cl^- ions already stuck on the surface, we will achieve of the second type of adsorption. Thus, the possible adsorption interactions of the inhibitor are illustrated in Fig. 13 in which its protonated form has the following form (Agrawal et al., 2021):



Conclusively, under acidic conditions, the steel surface develops anodic and cathodic active sites for corrosion. The functional groups containing N and O atoms can directly

undergo interactions between the unshared electron pair of the inhibitor and the vacant d orbital of the surface iron atoms. To adsorb the inhibitor onto the MS substrate, a chemisorption method involving evacuation of H_2O molecules from the metal substrate and electron exchange between the inhibitor heteroatoms and the iron atoms of the steel can be applied. The inhibitor molecule could potentially be adsorbed onto the metal substrate due to donor–acceptor interactions involving electrons from heterocyclic rings and vacant d-orbitals of the iron surface. On the other hand, proton molecules can adsorb directly onto the surface via Cl^- ions. This suggests that our studied corrosion inhibitor has excellent corrosion inhibition efficiency compared to some of the recent green corrosion inhibitors.

4. Conclusion

Our work demonstrates the anticorrosion performance and interfacial mechanism of a new carbocyclic compound (3-benzoyl-4-hydroxy-4-phenyl-2,6-(4-methylphenyl)cyclohexane-1,1-dicarbonitrile (MPC)) as an eco-friendly inhibitor for MS corrosion in 1 M HCl solution. The organic layer formed on MS surface using MPC inhibitor was beneficial for excellent corrosion protection of steel alloy. From the chemical, electrochemical, and computational results obtained throughout this work, the following conclusions can be drawn:

- MPC is the best candidate for corrosion protection behavior, which acts to inhibit both anodic and cathodic processes.
- On the basis of the temperature dependence, it was found that the inhibition performance of MPC was stable even at high temperatures and that its adsorption is accomplished by chemisorption interaction with respect to the Langmuir isotherm model.
- SEM-EDX analysis confirms the formation of an adhesive protective layer on the metallic surface.

- The formation of strong covalent bonds and intermolecular interactions were confirmed via DFTB and MD calculations through the parallel adsorption configurations.
- According to all the results, it was concluded that the interaction of MPC inhibitor on the metal surface would be optimized by electron transfer behavior from carbocyclic inhibitor and would be responsible for excellent electrochemical resistance.
- We believe that the electrochemical behavior as well as the interfacial mechanism of carbocyclic compound detailed in our research work will provide a reference for the development of future eco-friendly hybrid materials with excellent functional properties.

CRedit authorship contribution statement

Abdelkarim Chaouiki: Conceptualization, Methodology, Investigation, Writing – original draft. **Maryam Chafiq:** Data curation, Writing – original draft. **Aisha H. Al-Moubaraki:** Formal analysis, Investigation. **Mohamed Bakhouch:** Conceptualization. **Mohamed El Yazidi:** Conceptualization. **Young Gun Ko:** Supervision, Visualization.

Declaration of competing interest

The authors declare that they have no known competing financial interests or personal relationships that could have influenced the work reported in this study.

Acknowledgements

This work was supported by the Fundamental-Core National Project of the National Research Foundation (NRF) funded by the Ministry of Science and ICT, Republic of Korea (2022R1F1A1072739). The authors are thankful to innovation city staff of Sidi Mohamed Ben Abdellah University for spectroscopic measurement.

References

- Agrawal, R., Verma, A., Singhania, R.R., Varjani, S., Di Dong, C., Patel, A.K., 2021. Current understanding of the inhibition factors and their mechanism of action for the lignocellulosic biomass hydrolysis. *Bioresour. Technol.* 332, 125042.
- Alamry, K.A., Hussein, M.A., Musa, A., Haruna, K., Saleh, T.A., 2021. The inhibition performance of a novel benzenesulfonamide-based benzoxazine compound in the corrosion of X60 carbon steel in an acidizing environment. *RSC Adv.* 11, 7078–7095.
- Antonijevic, M., Petrovic, M., 2008. Copper corrosion inhibitors. A review. *Int J Electrochem Sci* 3, 1–28.
- Aradi, B., Hourahine, B., Frauenheim, T., 2007. DFTB+, a sparse matrix-based implementation of the DFTB method. *J. Phys. Chem. A* 111, 5678–5684.
- Assad, H., Kumar, A., 2021. Understanding functional group effect on corrosion inhibition efficiency of selected organic compounds. *J. Mol. Liq.* 344, 117755.
- Banerjee, G., Malhotra, S., 1992. Contribution to adsorption of aromatic amines on mild steel surface from HCl solutions by impedance, UV, and Raman spectroscopy. *Corrosion* 48, 10–15.
- Beniken, M., Salim, R., Ech-chihbi, E., Sfaira, M., Hammouti, B., Touhami, M.E., Mohsin, M., Taleb, M., 2022. Adsorption behavior and corrosion inhibition mechanism of a polyacrylamide on C-steel in 0.5 M H₂SO₄: Electrochemical assessments and molecular dynamic simulation. *J. Mol. Liq.* 348, 118022.

- Chafiq, M., Chaouiki, A., Al-Hadeethi, M.R., Salghi, R., Chung, I.-M., 2021a. A joint experimental and theoretical investigation of the corrosion inhibition behavior and mechanism of hydrazone derivatives for mild steel in HCl solution. *Colloids Surf. Physicochem. Eng. Asp.* 610, 125744.
- Chafiq, M., Chaouiki, A., Salghi, R., Tachallait, H., Bougrin, K., Ali, I.H., Siaj, M., 2021b. Adsorption mechanism of 3-(1, 4-disubstituted-1, 2, 3-triazolyl) uridine nucleosides against the corrosion of mild steel in HCl. *Mater. Chem. Phys.* 268, 124742.
- Chaouiki, A., Han, D.I., Ko, Y.G., 2022a. Computational molecular-level prediction of heterocyclic compound–metal surface interfacial behavior. *J. Colloid Interface Sci.*
- Chaouiki, A., Han, D.I., Ko, Y.G., 2022b. Computational molecular-level prediction of heterocyclic compound–metal surface interfacial behavior. *J. Colloid Interface Sci.* 622, 452–468.
- Chen, Y., Hong, T., Gopal, M., Jepson, W., 2000. EIS studies of a corrosion inhibitor behavior under multiphase flow conditions. *Corros. Sci.* 42, 979–990.
- Chigondo, M., Chigondo, F., 2016. Recent natural corrosion inhibitors for mild steel: an overview. *J. Chem.* 2016.
- Chugh, B., Singh, A.K., Thakur, S., Pani, B., Lgaz, H., Chung, I.-M., Jha, R., Ebenso, E.E., 2020. Comparative investigation of corrosion-mitigating behavior of thiazazole-derived bis-schiff bases for mild steel in acid medium: experimental, theoretical, and surface study. *ACS Omega* 5, 13503–13520.
- Dararatana, N., Seidi, F., Crespy, D., 2018. pH-sensitive polymer conjugates for anticorrosion and corrosion sensing. *ACS Appl. Mater. Interfaces* 10, 20876–20883.
- Dariva, C.G., Galio, A.F., 2014. Corrosion inhibitors—principles, mechanisms and applications. *Dev. Corros. Prot.* 16, 365–378.
- Desimone, M., Grundmeier, G., Gordillo, G., Simison, S., 2011. Amphiphilic amido-amine as an effective corrosion inhibitor for mild steel exposed to CO₂ saturated solution: polarization, EIS and PM-IRRAS studies. *Electrochimica Acta* 56, 2990–2998.
- Ebenso, E.E., Verma, C., Olasunkanmi, L.O., Akpan, E.D., Verma, D. K., Lgaz, H., Guo, L., Kaya, S., Quraishi, M.A., 2021. Molecular modelling of compounds used for corrosion inhibition studies: a review. *Phys. Chem. Chem. Phys.*
- Echihhi, S., Hsissou, R., Benzbiria, N., Afrok, M., Boudalia, M., Bellaouchou, A., Guenbour, A., Azzi, M., Tabyaoui, M., 2021. Performance of Methanolic Extract of Artemisia Herba Alba as a Potential Green Inhibitor on Corrosion Behavior of Mild Steel in Hydrochloric Acid Solution. *Biointerface Res Appl Chem* 11, 14751–14763.
- Elgaddafi, R., Ahmed, R., Shah, S., 2021. Corrosion of carbon steel in CO₂ saturated brine at elevated temperatures. *J. Pet. Sci. Eng.* 196, 107638.
- El-Sayed, M., 2007. Sherif, RM Erasmus and JD Comins, Effects of 3-amino-1, 2, 4-triazole on the inhibition of copper corrosion in acidic chloride solutions. *J. Colloid Interface Sci* 311, 144.
- Elstner, M., Porezag, D., Jungnickel, G., Elsner, J., Haugk, M., Frauenheim, T., Suhai, S., Seifert, G., 1998. Self-consistent-charge density-functional tight-binding method for simulations of complex materials properties. *Phys. Rev. B* 58, 7260.
- Fawzy, A., Farghaly, T.A., Al Bahir, A.A., Hameed, A.M., Alharbi, A., El-Ossaily, Y.A., 2021. Investigation of three synthesized propane bis-oxindoline derivatives as inhibitors for the corrosion of mild steel in sulfuric acid solutions. *J. Mol. Struct.* 1223, 129318.
- Gaber, G.A., Mohamed, L.Z., Järvenpää, A., Hamada, A., 2021. Enhancement of corrosion protection of AISI 201 austenitic stainless steel in acidic chloride solutions by Ce-doped TiO₂ coating. *Surf. Coat. Technol.* 423, 127618.
- Gerengi, H., Sahin, H.I., 2012. Schinopsis lorentzii extract as a green corrosion inhibitor for low carbon steel in 1 M HCl solution. *Ind. Eng. Chem. Res.* 51, 780–787.
- Golabadi, M., Aliofkhaezai, M., Toorani, M., 2021. Corrosion behavior of zirconium-pretreated/epoxy-coated mild steel: New approach for determination of cathodic disbondment resistance by

- electrochemical impedance spectroscopy. *J. Alloys Compd.* 873, 159800.
- Guo, Z., Hui, X., Zhao, Q., Guo, N., Yin, Y., Liu, T., 2021. Pigmented *Pseudoalteromonas piscicida* exhibited dual effects on steel corrosion: Inhibition of uniform corrosion and induction of pitting corrosion. *Corros. Sci.* 190, 109687.
- Guo, L., Qi, C., Zheng, X., Zhang, R., Shen, X., Kaya, S., 2017. Toward understanding the adsorption mechanism of large size organic corrosion inhibitors on an Fe (110) surface using the DFTB method. *RSC Adv.* 7, 29042–29050.
- Haris, N.I.N., Sobri, S., Yusof, Y.A., Kassim, N.K., 2020. An overview of molecular dynamic simulation for corrosion inhibition of ferrous metals. *Metals* 11, 46.
- Humphrey, W., Dalke, A., Schulten, K., 1996. VMD: visual molecular dynamics. *J. Mol. Graph.* 14, 33–38.
- Iroha, N.B., Madueke, N., Mkpenie, V., Ogunyemi, B., Nnanna, L.A., Singh, S., Akpan, E.D., Ebenso, E.E., 2021. Experimental, adsorption, quantum chemical and molecular dynamics simulation studies on the corrosion inhibition performance of Vincamine on J55 steel in acidic medium. *J. Mol. Struct.* 1227, 129533.
- Jacobsen, N.E., 2016. NMR data interpretation explained: understanding 1D and 2D NMR spectra of organic compounds and natural products. John Wiley & Sons.
- Jiao, X., Fu, W., Shao, W., Zhu, X., Zhou, Y., Xing, X., Wang, Z., Yang, Q., 2021. First-principles calculation on γ -Fe/La2O3 interface properties and austenite refinement mechanism by La2O3. *Mater. Chem. Phys.* 259, 124194.
- Joseph, O.O., Joseph, O.O., 2021. Corrosion Inhibition of Aluminium Alloy by Chemical Inhibitors: An Overview. IOP Publishing 012170.
- Lebrini, M., Lagrenee, M., Vezin, H., Gengembre, L., Bentiss, F., 2005. Electrochemical and quantum chemical studies of new thiadiazole derivatives adsorption on mild steel in normal hydrochloric acid medium. *Corros. Sci.* 47, 485–505.
- Li, X., Deng, S., Fu, H., 2010. Adsorption and inhibition effect of vanillin on cold rolled steel in 3.0 M H3PO4. *Prog. Org. Coat.* 67, 420–426.
- Lu, T., Chen, F., 2012. Multiwfn: a multifunctional wavefunction analyzer. *J. Comput. Chem.* 33, 580–592.
- Luo, Y., Zhang, Q., Zhang, R., Tang, G., Guo, L., n.d. Insight into the Oxygen Adsorption Behaviors of Graphene Coated Fe (1 1 0) Surface: Dftb Investigations. Available SSRN 4098275.
- Martinez, S., Stern, I., 2002. Thermodynamic characterization of metal dissolution and inhibitor adsorption processes in the low carbon steel/mimosa tannin/sulfuric acid system. *Appl. Surf. Sci.* 199, 83–89.
- Migahed, M., El-Rabie, M., Nady, H., Zaki, E., 2018. Novel Gemini cationic surfactants as anti-corrosion for X-65 steel dissolution in oilfield produced water under sweet conditions: Combined experimental and computational investigations. *J. Mol. Struct.* 1159, 10–22.
- Mobin, M., Zehra, S., Aslam, R., 2016. L-Phenylalanine methyl ester hydrochloride as a green corrosion inhibitor for mild steel in hydrochloric acid solution and the effect of surfactant additive. *RSC Adv.* 6, 5890–5902.
- Mofidabadi, A.H.J., Dehghani, A., Ramezanzadeh, B., 2022. Sinapis arvensis (Mustard) extract derived bio-molecules linked Zinc-II ions; Integrated electrochemical & surface investigations. *J. Mol. Liq.* 346, 117085.
- Mousavi, S.A., Pitchumani, R., 2022. Bioinspired nonwetting surfaces for corrosion inhibition over a range of temperature and corrosivity. *J. Colloid Interface Sci.* 607, 323–333.
- Musa, A.Y., Jalgham, R.T., Mohamad, A.B., 2012. Molecular dynamic and quantum chemical calculations for phthalazine derivatives as corrosion inhibitors of mild steel in 1 M HCl. *Corros. Sci.* 56, 176–183.
- Noor, E.A., Al-Moubaraki, A.H., 2008. Thermodynamic study of metal corrosion and inhibitor adsorption processes in mild steel/1-methyl-4 [4(-X)-styryl pyridinium iodides/hydrochloric acid systems. *Mater. Chem. Phys.* 110, 145–154.
- Obot, I., Onyeachu, I.B., Umoren, S.A., Quraishi, M.A., Sorour, A.A., Chen, T., Aljeaban, N., Wang, Q., 2020. High temperature sweet corrosion and inhibition in the oil and gas industry: Progress, challenges and future perspectives. *J. Pet. Sci. Eng.* 185, 106469.
- Onyeachu, I.B., Obot, I.B., Sorour, A.A., Abdul-Rashid, M.I., 2019. Green corrosion inhibitor for oilfield application I: electrochemical assessment of 2-(2-pyridyl) benzimidazole for API X60 steel under sweet environment in NACE brine ID196. *Corros. Sci.* 150, 183–193.
- Prasad, Y.R., Rao, A.L., Rambabu, R., 2008. Synthesis and antimicrobial activity of some chalcone derivatives. *E-J. Chem.* 5, 461–466.
- Qiang, Y., Guo, L., Li, H., Lan, X., 2021. Fabrication of environmentally friendly Losartan potassium film for corrosion inhibition of mild steel in HCl medium. *Chem. Eng. J.* 406, 126863.
- Quraishi, M., Chauhan, D.S., Ansari, F.A., 2021. Development of environmentally benign corrosion inhibitors for organic acid environments for oil-gas industry. *J. Mol. Liq.* 329, 115514.
- Shaban, S.M., Elbhrawy, M., Fouda, A., Rashwan, S., Ibrahim, H.E., Elsharif, A.M., 2021. Corrosion inhibition and surface examination of carbon steel 1018 via N-(2-(2-hydroxyethoxy) ethyl)-N, N-dimethyloctan-1-aminium bromide in 1.0 M HCl. *J. Mol. Struct.* 1227, 129713.
- Sharma, S., Kumar, A., 2021. Recent advances in metallic corrosion inhibition: A review. *J. Mol. Liq.* 322, 114862.
- Sherif, E., Park, S.-M., 2006. 2-Amino-5-ethyl-1, 3, 4-thiadiazole as a corrosion inhibitor for copper in 3.0% NaCl solutions. *Corros. Sci.* 48, 4065–4079.
- Singh, W.P., Bockris, J., 1996. Toxicity issues of organic corrosion inhibitors: applications of QSAR model. *OnePetro*.
- Solmaz, R., 2010. Investigation of the inhibition effect of 5-((E)-4-phenylbuta-1, 3-dienylideneamino)-1, 3, 4-thiadiazole-2-thiol Schiff base on mild steel corrosion in hydrochloric acid. *Corros. Sci.* 52, 3321–3330.
- Stupnišek-Lisac, E., Božić, A.L., Cafuk, I., 1998. Low-toxicity copper corrosion inhibitors. *Corrosion* 54, 713–720.
- Stupnišek-Lisac, E., Gazivoda, A., Madžarac, M., 2002. Evaluation of non-toxic corrosion inhibitors for copper in sulphuric acid. *Electrochimica Acta* 47, 4189–4194.
- Tian, H., Li, W., Hou, B., Wang, D., 2017. Insights into corrosion inhibition behavior of multi-active compounds for X65 pipeline steel in acidic oilfield formation water. *Corros. Sci.* 117, 43–58.
- Topçu, İ.B., Uzunömeroğlu, A., 2020. Properties of corrosion inhibitors on reinforced concrete. *J Struct Eng Appl Mech* 3, 93–109.
- Verma, D.K., Kaya, S., Ech-chihbi, E., El-Hajjaji, F., Phukan, M. M., Alnashiri, H.M., 2021b. Investigations on some coumarin based corrosion inhibitors for mild steel in aqueous acidic medium: Electrochemical, surface morphological, density functional theory and Monte Carlo simulation approach. *J. Mol. Liq.* 329, 115531.
- Verma, C., Quraishi, M., Alfantazi, A., Rhee, K.Y., 2021a. Corrosion inhibition potential of chitosan based Schiff bases: Design, performance and applications. *Int. J. Biol. Macromol.* 184, 135–143.
- Wang, X., Wang, B., Wang, Q., Li, R., Liu, H., Jiang, H., Liu, J., 2021. Inhibition effect and adsorption behavior of two pyrimidine derivatives as corrosion inhibitors for Q235 steel in CO₂-saturated chloride solution. *J. Electroanal. Chem.* 903, 115827.
- Zaferani, S.H., Sharifi, M., Zaarei, D., Shishesaz, M.R., 2013. Application of eco-friendly products as corrosion inhibitors for metals in acid pickling processes—A review. *J. Environ. Chem. Eng.* 1, 652–657.
- Zaidon, F.H., Kassim, K., Zaki, H.M., Embong, Z., Hashim, N.Z.N., 2021. Adsorption and corrosion inhibition accomplishment for thiosemicarbazone derivatives for mild steel in 1.0 M HCl medium: Electrochemical, XPS and DFT studies. *J. Mol. Liq.* 329, 115553.

- Zhang, G., Cheng, Y., 2009. On the fundamentals of electrochemical corrosion of X65 steel in CO₂-containing formation water in the presence of acetic acid in petroleum production. *Corros. Sci.* 51, 87–94.
- Zhang, Q.H., Jiang, Z.N., Li, Y.Y., Wang, X., Xiong, W., Liu, H.F., Zhang, G.A., 2022. In-depth insight into the inhibition mechanism of the modified and combined amino acids corrosion inhibitors: “intramolecular synergism” vs. “intermolecular synergism”. *Chem. Eng. J.* 135439.
- Zhang, Z., Wang, Q., Wang, X., Gao, L., 2017. The influence of crystal faces on corrosion behavior of copper surface: First-principle and experiment study. *Appl. Surf. Sci.* 396, 746–753.
- Zheng, G., Witek, H.A., Bobadova-Parvanova, P., Irle, S., Musaev, D. G., Prabhakar, R., Morokuma, K., Lundberg, M., Elstner, M., Köhler, 2007. Parameter calibration of transition-metal elements for the spin-polarized self-consistent-charge density-functional tight-binding (DFTB) method: Sc, Ti, Fe Co, and Ni. *J. Chem. Theory Comput.* 3, 1349–1367.
- Zhong, X., Li, M., Zhou, B., Yao, M., Shen, J., 2021. In-situ electrochemical impedance spectroscopy investigations on the early stage corrosion behavior of Zircaloy-4 in high-temperature lithiated water. *Corros. Sci.* 182, 109223.
- Zhu, M., He, Z., Guo, L., Zhang, R., Anadebe, V.C., Obot, I.B., Zheng, X., 2021. Corrosion inhibition of eco-friendly nitrogen-doped carbon dots for carbon steel in acidic media: performance and mechanism investigation. *J. Mol. Liq.* 342, 117583.